

CERN-EP-2016-129
20 May 2016

**Measurement of azimuthal correlations of D mesons and charged particles
in pp collisions at $\sqrt{s} = 7$ TeV and p–Pb collisions at $\sqrt{s_{NN}} = 5.02$ TeV**

ALICE Collaboration*

Abstract

The azimuthal correlations of D mesons and charged particles were measured with the ALICE detector in pp collisions at $\sqrt{s} = 7$ TeV and p–Pb collisions at $\sqrt{s_{NN}} = 5.02$ TeV at the Large Hadron Collider. D^0 , D^+ , and D^{*+} mesons with transverse momentum $3 < p_T < 16$ GeV/ c and rapidity in the nucleon-nucleon centre-of-mass system $|y_{cms}| < 0.5$ (pp collisions) and $-0.96 < y_{cms} < 0.04$ (p–Pb collisions) were correlated to charged particles with $p_T > 0.3$ GeV/ c . The properties of the correlation peak induced by the jet containing the D meson, described in terms of the yield of charged particles in the peak and peak width, are compatible within uncertainties between the two collision systems, and described by Monte-Carlo simulations based on the PYTHIA and POWHEG event generators.

© 2016 CERN for the benefit of the ALICE Collaboration.
Reproduction of this article or parts of it is allowed as specified in the CC-BY-4.0 license.

*See Appendix A for the list of collaboration members

1 Introduction

The study of the azimuthal correlation of D mesons and charged particles produced in a proton-proton (pp) collision provides a way to characterize charm production and fragmentation processes. Perturbative QCD calculations relying on the collinear-factorisation approach, like FONLL [1] and GM-VFNS [2], or based on the k_T -factorisation approach [3] describe reasonably well within the uncertainties the transverse-momentum (p_T)-differential production cross sections of D mesons from charm-quark fragmentation (referred to as “prompt” D mesons) measured at central rapidity (y) using the ALICE detector [4, 5]. Though these calculations represent the state of the art for the computation of (p_T, y) -differential cross sections of charm quarks and charmed hadrons, the kinematic relationship between D mesons and particles from charm fragmentation and from the underlying event is accessible only with event generators coupled with parton-shower Monte-Carlo programs like those provided by PYTHIA [6] and HERWIG [7]. The order of hard-scattering matrix elements used, the specific implementation of parton shower and hadronisation, as well as the modeling of the underlying event have an influence on the angular correlations of D mesons and charged particles produced in the event.

For events with a charm quark-antiquark pair produced back-to-back in azimuth, as in leading order (LO) QCD processes, the angular correlation of D mesons and charged particles (i.e. the distribution of the differences of the azimuthal angles, $\Delta\phi = \phi_{\text{ch}} - \phi_{\text{D}}$, and pseudorapidities, $\Delta\eta = \eta_{\text{ch}} - \eta_{\text{D}}$) features a “near-side” peak around $(\Delta\phi, \Delta\eta) = (0, 0)$, originating from the jet containing the “trigger” D meson, and an “away-side” peak around $\Delta\phi = \pi$, generated by the recoiling jet, which can also include the decay products of the other charmed hadron produced in the collision. The away-side peak extends over a wide range in $\Delta\eta$. The two peaks lie on top of an approximately flat distribution deriving from the correlation of D mesons with charged particles from the underlying event. Next-to-leading order (NLO) production processes can give rise to significantly different correlation patterns [8, 9]. For example, the radiation of a hard gluon from a charm quark can smear the back-to-back topology of LO production and broaden both the near- and the away-side peak. In addition, quark-antiquark charm pairs originated from the splitting of a gluon can be rather collimated and, especially at high p_T , may generate sprays of hadrons contributing to a unique and broader “near-side” peak of the azimuthal correlation of D mesons and charged particles. This may also result in a broadening of the away-side peak due to the contribution of associated particles coming from the fragmentation of the recoiling parton (typically a gluon or a light quark). Finally, for hard-scattering topologies classified as “flavour excitation” (see e.g. [9]), in which a charm quark (antiquark) from an initial splitting $g \rightarrow c\bar{c}$ undergoes a hard interaction, the hadrons originating from the antiquark (quark) can be significantly separated in rapidity with respect to the trigger D meson and contribute with a rather flat term to the $\Delta\phi$ -correlation distribution.

Correlations between D mesons were measured at the LHC in pp collisions at $\sqrt{s} = 7$ TeV [10], providing information on charm production mechanisms and on the properties of events containing heavy flavours. Azimuthal correlations of electrons from heavy-flavour hadron decays and charged particles were also exploited to study the relative beauty contribution to the population of electrons from heavy-flavour hadron decays in pp collisions at RHIC and at the LHC [11, 12]. Finally, two-particle azimuthal correlations play a crucial role in the investigation of the modification of jet-production properties in relativistic heavy-ion collisions, at both RHIC and LHC energies [13–15]. The observation of the suppression of the away-side correlation peak was ascribed to partonic in-medium energy loss, providing important constraints to the dependence of the energy loss on the distance covered by partons in the Quark Gluon Plasma (QGP) formed in these collisions. The measurements of azimuthal correlations in pp and p–Pb collisions serve as a reference to quantify possible modifications in Pb–Pb collisions.

The angular distribution of particles produced in an event is sensitive to collective effects that correlate particle production over wide phase-space regions. This is particularly relevant in Pb–Pb collisions with non-zero collision impact parameter, where the azimuthal asymmetry of the overlapping region of the colliding nuclei gives rise to anisotropic pressure gradients inducing an anisotropy in the azimuthal

distribution of particle momenta [16, 17]. The main component of the Fourier decomposition used to describe the resulting $\Delta\phi$ distribution of two particle correlations is the 2nd order term, proportional to $\cos(2\Delta\phi)$, called elliptic flow or v_2 . Given that correlations induced by the collective motion of the system extend over large pseudorapidity ranges, the elliptic-flow term manifest itself with the presence of two long-range ridge-like structures in the near and away sides of two-particle angular correlations. Unexpectedly, similar long-range correlation structures were observed in high-multiplicity pp and p–Pb collisions at the LHC [18–23]. Also in central d–Au collisions at RHIC [24, 25] similar results were obtained, although contributions from jet-like correlations due to biases on the event selection could not be excluded [26]. The origin of such v_2 -like structures is still debated. Positive v_2 values in high-multiplicity pp collisions and p–Pb (d–Au) collisions at LHC (RHIC) are expected in models including final-state effects [27–31], as well as initial-state effects related to the Color Glass Condensate [32] or to gluon bremsstrahlung by a quark-antiquark string [33]. A modification of the azimuthal correlations of D mesons and charged particles in p–Pb with respect to pp collisions could be a signal of the presence of long-range v_2 -like correlations also for particles originating from hard-scattering processes, complementing the information obtained from correlations of light-flavour particles, which, at low p_T , are mostly produced in soft processes. The D-meson p_T -differential production cross section in p–Pb collisions at $\sqrt{s_{NN}} = 5.02$ TeV was measured with the ALICE experiment in the interval of rapidity in the nucleon-nucleon centre-of-mass system $-0.96 < y_{cms} < 0.04$ [34]. The data are compatible, within uncertainties, with a Glauber-model-based geometrical scaling of a pp collision reference obtained from the cross sections measured at $\sqrt{s} = 7$ TeV and $\sqrt{s} = 2.76$ TeV. This observation suggests that, in p–Pb collisions, nuclear effects are rather small for D mesons in the $1 < p_T < 24$ GeV/ c range of the measurement. However, they could still affect angular correlations as observed at RHIC for azimuthally-correlated pairs of electrons and muons from decays of heavy-flavour hadrons in d–Au collisions at $\sqrt{s_{NN}} = 200$ GeV [35]. A modification of the azimuthal correlation of heavy-flavour particles in p–Pb collisions could be expected at the LHC due to gluon saturation in the heavy nucleus [36]. Moreover, transport models based on the Langevin equation [37, 38] can describe, within uncertainties, the nuclear modification factor of D mesons measured in p–Pb collisions at the LHC and that of electrons from heavy-flavour hadron decays measured in d–Au collisions at RHIC [39]. These models assume the formation of a small-size QGP in p–Pb and d–Au collisions and include the possibility of heavy-flavour hadron formation via coalescence of heavy quarks with thermalized light quarks from the medium. These transport calculations predict a positive D-meson v_2 in central p–Pb collisions. As an example, in the case of the POWLANG model [37] the maximum expectation for the 20% most central p–Pb collisions is $v_2 \sim 5\%$ at $p_T = 4$ GeV/ c . A finite v_2 of muons from heavy-flavour hadron decays in high-multiplicity p–Pb collisions was also suggested in [21] as one of the possibilities for reconciling the measured values of v_2 of inclusive muons with the expectations based on the multi-phase transport model AMPT [40].

In this paper we report the first measurements of azimuthal correlations of prompt D mesons and charged primary particles in pp and p–Pb collisions at $\sqrt{s} = 7$ TeV and $\sqrt{s_{NN}} = 5.02$ TeV, respectively. In what follows, primary particles are defined as particles originated at the collision point, including those deriving from strong and electromagnetic decays of unstable particles, and those from decays of hadrons with charm or beauty. The paper is organized as follows. In Section 2 the data samples used and the details of the ALICE experimental apparatus relevant for this analysis are described. The analysis strategy, the D-meson signal extraction, the associated-track selection criteria, and the corrections applied to measure the correlations between D mesons and charged primary particles are reported in Section 3. In the same section, the fit procedure adopted to quantify the correlation peak properties is described. Section 4 reports the systematic uncertainties affecting the measurement. The results are discussed in Section 5. The paper is then concluded by a summary.

2 Experimental apparatus and data samples

2.1 The ALICE detector and event selection

The ALICE apparatus [41, 42] consists of a central barrel embedded in a 0.5 T solenoidal magnetic field, a forward muon spectrometer, and a set of detectors located in the forward- and backward-rapidity regions dedicated to trigger and event characterization. The analysis reported in this paper is performed with the central barrel detectors. Charged tracks are reconstructed with the Inner Tracking System (ITS), consisting of six layers of silicon detectors, and the Time Projection Chamber (TPC). Particle identification (PID) is based on the specific energy loss dE/dx in the TPC gas and on the time of flight from the interaction vertex to the Time Of Flight (TOF) detector. The ITS, TPC and TOF detectors provide full azimuthal coverage in the pseudorapidity interval $|\eta| < 0.9$.

The pp data sample consists of about $3 \cdot 10^8$ minimum-bias events, corresponding to an integrated luminosity of $L_{\text{int}} = 5 \text{ nb}^{-1}$. These collisions are triggered by the presence of at least one hit in one of the V0 scintillator arrays, covering the ranges $-3.7 < \eta < -1.7$ and $2.8 < \eta < 5.1$, or in the Silicon Pixel Detector (SPD), constituting the two innermost layers of the ITS, with an acceptance of $|\eta| < 2$ (inner layer) and $|\eta| < 1.4$ (outer layer). The p–Pb data sample consists of about 10^8 minimum-bias events, corresponding to an integrated luminosity of about $L_{\text{int}} = 50 \mu\text{b}^{-1}$. In this case the minimum-bias trigger requires signals in both the V0 detectors.

Only events with a reconstructed primary interaction vertex within ± 10 cm from the centre of the detector along the beam line are considered for both pp and p–Pb collisions. For p–Pb collisions, the center-of-mass reference frame of the nucleon-nucleon collision is shifted in rapidity by $\Delta y_{\text{NN}} = 0.465$ in the proton direction with respect to the laboratory frame, due to the different per-nucleon energies of the proton and the lead beams.

Beam-gas events are removed by offline selections based on the timing information provided by the V0 and the Zero Degree Calorimeters (two sets of neutron and proton calorimeters located around 110 m from the interaction point along the beam direction), and the correlation between the number of hits and track segments in the SPD detector.

The minimum-bias trigger efficiency is 100% for events with D mesons with $p_{\text{T}} > 1 \text{ GeV}/c$ for both pp and p–Pb data sets. For the analyzed data samples, the probability of pile-up from collisions in the same bunch crossing is below 4% per triggered pp event and below the per-cent level per triggered p–Pb event. Events in which more than one primary interaction vertex is reconstructed with the SPD detector are rejected, which effectively removes the impact of in-bunch pile-up events on the analysis. The contribution of particles from pile-up of pp collisions in different bunch crossings is also negligible due to the selections applied to the tracks used in this analysis and the large interval between subsequent bunch crossings in the data samples used.

2.2 Monte Carlo simulations

Monte-Carlo simulations including a complete description of the ALICE detector are used to calculate the corrections for the azimuthal-correlation distributions evaluated from data. The luminous region distribution, the conditions of all the ALICE detectors, and their evolution with time during the pp and p–Pb collision runs are taken into account in the simulations. Proton-proton collisions are simulated with the PYTHIA 6.4.21 event generator [6] with the Perugia-0 tune (tune number 320) [43] while p–Pb collisions are simulated using the HIJING v1.36 event generator [44]. For the calculation of D-meson reconstruction efficiencies PYTHIA simulations of pp collisions are used, requiring in each event the creation of a $c\bar{c}$ or $b\bar{b}$ pair. In the simulation used for the analysis of p–Pb data, an event from a p–Pb collision simulated with HIJING is added on top of the PYTHIA event. The generated particles are transported through the detector with the GEANT3 transport package [45].

The measured correlation distributions are compared to simulation results obtained with the event generators PYTHIA 6.4.25 [6] (tunes number 320, 327, and 350, corresponding to the reference versions of the Perugia-0, Perugia-2010, and Perugia-2011 sets [43], respectively), PYTHIA 8.1 (tune 4C) [46], and POWHEG [47, 48] coupled to PYTHIA (Perugia-2011 tune). PYTHIA simulations utilise LO-pQCD matrix elements for $2 \rightarrow 2$ processes, along with a leading-logarithmic p_T -ordered parton shower, the Lund string model for hadronisation, and an underlying-event simulation including Multiple-Parton Interactions (MPI). With respect to older tunes, the Perugia tunes use different initial-state radiation and final-state radiation models. One of the main differences is that the parton shower algorithm is based on a p_T -ordered evolution rather than a virtuality-ordered one. Significant differences in the treatment of colour reconnection, MPI, and the underlying event were also introduced. Perugia 0 is the first of the series. The Perugia-2010 tunes differ from the Perugia-0 ones in the amount of final-state radiation and by a modification of the high- z fragmentation (inducing a slight hardening of the spectra). They are expected to better reproduce observables related to the jet shape. For the Perugia-2011 tunes first LHC data, mainly from multiplicity and underlying-event related measurements, were considered. PYTHIA 8.1 is the rewrite in C++ of PYTHIA 6, written in Fortran, and includes also several improvements in the treatment of MPI and colour reconnection [46]. In the simulations performed at $\sqrt{s} = 5.02$ TeV, the centre-of-mass frame is boosted in rapidity by $\Delta_{y_{NN}} = 0.465$ in order to reproduce the rapidity shift of the reference frame of the nucleon-nucleon collision in the p–Pb collision system.

POWHEG is a NLO-pQCD generator [47, 48] that, coupled to parton shower programs (e.g. from PYTHIA or HERWIG [7]), can provide exclusive final-state particles, maintaining the next-to-leading order accuracy for inclusive observables. The charm-production cross sections obtained with POWHEG+PYTHIA are consistent with FONLL [1] and GM-VFNS [2] calculations within the respective uncertainties, and in agreement with measured D-meson production cross sections within the model and experimental uncertainties [49, 50]. The POWHEG+PYTHIA simulations presented in this paper are obtained with the POWHEG BOX framework [51, 52] and the tune Perugia 2011 of PYTHIA 6.4.25. For the comparison with the measured p–Pb collision data, parton distribution functions (PDFs) corrected for nuclear effects (CT10nlo [53] with EPS09 [54]) are used. Before passing them to the PYTHIA parton shower, the scattered partons are boosted in rapidity by $\Delta_{y_{NN}} = 0.465$.

3 Data analysis

3.1 D-meson and associated-particle reconstruction

The correlation analysis is performed by associating D mesons (D^0 , D^+ , D^{*+} mesons and their antiparticles), defined as “trigger” particles, with charged primary particles in the same event, excluding those coming from the decay of the trigger D mesons themselves. The D^0 , D^+ , D^{*+} mesons and their charge conjugates are reconstructed via their hadronic decay channels $D^0 \rightarrow K^- \pi^+$, with Branching Ratio (BR) of $(3.88 \pm 0.05)\%$, $D^+ \rightarrow K^- \pi^+ \pi^+$, BR of $(9.13 \pm 0.19)\%$, and $D^{*+} \rightarrow D^0 \pi^+$, BR of $(67.7 \pm 0.5)\%$ [55]. The extraction of the D-meson signal is based on the reconstruction of decay vertices displaced from the primary vertex by a few hundred μm and on the identification of the decay-particle species. The same selection procedures used for the measurements of D-meson production in pp and p–Pb collisions at $\sqrt{s} = 7$ TeV and $\sqrt{s_{NN}} = 5.02$ TeV, respectively, are adopted [4, 34]. For both the pp and p–Pb data sets, D^0 and D^+ candidates are formed by combining tracks with $|\eta| < 0.8$ and $p_T > 0.3$ GeV/ c , which are required to have at least 70 out of a maximum of 159 possible associated space points in the TPC, a χ^2/NDF of the momentum fit in the TPC smaller than 2, and at least 2 out of 6 associated hits in the ITS. D^{*+} candidates are formed combining D^0 candidates with tracks with one point in the SPD, $|\eta| < 0.8$ and $p_T > 0.1$ GeV/ c . The main variables used to reject the combinatorial background are the separation between primary and secondary vertices, the distance of closest approach (DCA) of the decay tracks to the primary vertex, and the angle between the reconstructed D-meson momentum and the flight line defined by the primary and secondary vertices. A tighter selection is

applied for p–Pb collisions with respect to pp collisions to reduce the larger combinatorial background. The identification of charged kaons and pions is done using TPC and TOF detectors. A $\pm 3\sigma$ cut around the expected value for pions and kaons is applied on both TPC and TOF signals. The D mesons are selected in a fiducial rapidity range varying from $|y_{\text{lab}}| < 0.5$ at low p_T to $|y_{\text{lab}}| < 0.8$ for D mesons with $p_T > 5$ GeV/ c in order to avoid cases in which the decay tracks are close to the edge of the detector, where the acceptance decreases steeply. The D^0 and D^+ raw yields are extracted using fits to the distributions of invariant mass $M(K^-\pi^+)$ and $M(K^-\pi^+\pi^+)$, respectively, with a function composed of a Gaussian term for the signal and an exponential term modeling the combinatorial background. In the case of the D^{*+} , the raw yield is obtained with fits to the invariant-mass difference $\Delta M = M(K^-\pi^+\pi^+) - M(K^-\pi^+)$, using a Gaussian function for the signal and a threshold function multiplied by an exponential ($a\sqrt{\Delta M - M_\pi} \cdot e^{b(\Delta M - M_\pi)}$) to describe the background. Relatively wide D-meson p_T intervals ($3 < p_T < 5$ GeV/ c , $5 < p_T < 8$ GeV/ c , $8 < p_T < 16$ GeV/ c for pp collisions and $5 < p_T < 8$ GeV/ c , $8 < p_T < 16$ GeV/ c for p–Pb collisions) are chosen to reduce the statistical fluctuations in the azimuthal-correlation distributions. The statistical uncertainty of the D-meson raw yields in these p_T intervals varies from about 5% to 8% (3% to 5%) in pp (p–Pb) collisions for the D^0 and D^+ mesons and from about 5% to 6% (5% to 10%) for the D^{*+} mesons, depending on p_T . For both collision systems, the signal over background ratio of the signal peaks is between 0.2 and 1 for the D^0 and D^+ mesons, and up to 2.6 for the D^{*+} meson. In the interval $3 < p_T < 5$ GeV/ c the D-meson yield can be extracted from the invariant mass distribution with statistical uncertainty smaller than 3% in both pp and p–Pb collisions. However, in the latter case, the near- and away-side peaks of the azimuthal-correlation distribution, that have a small amplitude at low D-meson p_T , cannot be disentangled from the statistical fluctuations of the baseline, which is related to the multiplicity of the event and thus higher in p–Pb than in pp collisions. Therefore, for this p_T interval, the results are shown only for pp collisions.

Associated particles are defined as all charged primary particles with $p_T^{\text{assoc}} > 0.3$ GeV/ c and with pseudorapidity $|\eta| < 0.8$, except for the decay products of the trigger D meson. Particles coming from other weak decays or originating from interactions with the detector material are defined as secondary particles and are discarded. Reconstructed tracks with at least 70 points in the TPC and 3 in the ITS, and a χ^2/NDF of the momentum fit in the TPC smaller than 2 are associated to D-meson candidates. As estimated with Monte Carlo simulations (see Section 2.2), with this selection the track-reconstruction efficiency for charged primary particles in the pseudorapidity range $|\eta| < 0.8$ has an average value of about 85% in the interval $0.3 < p_T < 24$ GeV/ c , with variations contained within $\approx 5\%$ for $p_T < 1.5$ GeV/ c . Negligible variations are observed at higher p_T . The contamination of secondary particles is removed by requiring the DCA of the associated tracks to the primary vertex to be less than 2.5 mm in the transverse (x, y) plane and less than 1 cm along the beam line (z direction). This selection identifies primary particles with a purity (p_{prim}) of approximately 96% and with an efficiency higher than 99%, also for particles originating from decays of charm or beauty hadrons, which can be displaced by several hundred micrometers from the primary vertex. The purity is independent of p_T in the measured p_T range. For the D^0 -meson case, the low- p_T pion produced from the $D^{*+} \rightarrow D^0\pi^+$ decay is removed from the sample of associated particles by rejecting tracks that yield a ΔM compatible within 3σ with the value expected for D^{*+} mesons. It was verified with Monte Carlo simulations that this selection rejects more than 99% of the pions from D^{*+} decays in all D-meson p_T intervals considered and has an efficiency larger than 99% for primary particles with $p_T > 0.3$ GeV/ c .

3.2 Azimuthal-correlation distributions and corrections

D-meson candidates with invariant mass (M) in the range $|M - \mu| < 2\sigma$ (peak region), where μ and σ denote the mean and width of the Gaussian term of the invariant-mass fit function, are correlated to tracks selected with the criteria described above, and the difference in the azimuthal angle ($\Delta\phi$) and in pseudorapidity ($\Delta\eta$) of each pair is computed. In order to correct for the acceptance and reconstruction efficiency ($\text{Acc} \times \varepsilon$) of the associated tracks and for the variation of ($\text{Acc} \times \varepsilon$) of prompt D mesons

inside a given p_T interval, a weight equal to the inverse of the product of both ($\text{Acc} \times \varepsilon$) is assigned to each pair. The dependence of the associated-track efficiency on transverse momentum, pseudorapidity, and position of the primary vertex along the beam axis is taken into account. The dependence of the track reconstruction efficiency on the event multiplicity is negligible and therefore neglected. The reconstruction efficiency of prompt D mesons is calculated as a function of p_T and event multiplicity. It is of the order of few percent in the lower D-meson p_T interval, about 20% at high p_T [4, 34], and it varies within each p_T interval by up to a factor 2-3 (1.5-2) at low (high) p_T , depending on the D-meson species and collision system. The D-meson ($\text{Acc} \times \varepsilon$) factor accounts also for the p_T -dependent fiducial rapidity range of the selected D mesons (Sec. 3.1) in order to normalize the results to one unit of rapidity.

The obtained distribution, $C(\Delta\varphi, \Delta\eta)_{\text{peak}}$, includes the angular correlation of background D-meson candidates in the peak range. This contribution is estimated via the per-trigger correlation distribution of background candidates, $1/B_{\text{sidebands}} \times C(\Delta\varphi, \Delta\eta)_{\text{sidebands}}$, where $B_{\text{sidebands}}$ is the amount of background in the sideband invariant-mass range $4\sigma < |M - \mu| < 8\sigma$ (right side only, $4\sigma < M - \mu < 8\sigma$, in the case of D^{*+} mesons). The term $C(\Delta\varphi, \Delta\eta)_{\text{sidebands}}$ represents the correlation distribution obtained as described above, but selecting D-meson candidates with invariant mass in the sidebands. The background contribution is then subtracted from $C(\Delta\varphi, \Delta\eta)_{\text{peak}}$ after being normalized to the amount of background in the peak region, B_{peak} . The latter is obtained from the counts in the invariant-mass distribution in the peak region, after subtracting the signal, S_{peak} , estimated from the invariant-mass fit. Note that S_{peak} , B_{peak} and $B_{\text{sidebands}}$ are calculated from the invariant-mass distributions weighted by the inverse of the prompt D-meson reconstruction efficiency.

The correlation distributions $C(\Delta\varphi, \Delta\eta)_{\text{peak}}$ and $C(\Delta\varphi, \Delta\eta)_{\text{sidebands}}$ are corrected for the limited detector acceptance and detector spatial inhomogeneities using the event mixing technique. In this approach, D-meson candidates found in a given event are correlated with charged tracks from other events with similar multiplicity and position of the primary vertex along the beam axis. The distribution obtained from the mixed events, $\text{ME}(\Delta\varphi, \Delta\eta)$, shows a typical triangular shape as a function of $\Delta\eta$, due to the limited η coverage of the detector, and is approximately flat as a function of $\Delta\varphi$. The event-mixing distribution is rescaled by its average value in the range ($-0.2 < \Delta\varphi < 0.2, -0.2 < \Delta\eta < 0.2$) and its inverse is used as a map to weight the distributions $C(\Delta\varphi, \Delta\eta)_{\text{peak}}$ and $C(\Delta\varphi, \Delta\eta)_{\text{sidebands}}$. A correction for the purity of the primary-particle sample (p_{prim} , see Sec.3.1) is applied and the per-trigger normalization is obtained dividing by S_{peak} . The above procedure is summarized in the following Equation 1, where the notation \tilde{C} refers to angular-correlation distributions normalized by the number of trigger particles:

$$\tilde{C}_{\text{inclusive}}(\Delta\varphi, \Delta\eta) = \frac{p_{\text{prim}}}{S_{\text{peak}}} \left(\frac{C(\Delta\varphi, \Delta\eta)}{\text{ME}(\Delta\varphi, \Delta\eta)} \Big|_{\text{peak}} - \frac{B_{\text{peak}}}{B_{\text{sidebands}}} \frac{C(\Delta\varphi, \Delta\eta)}{\text{ME}(\Delta\varphi, \Delta\eta)} \Big|_{\text{sidebands}} \right), \quad (1)$$

$$\text{ME}(\Delta\varphi, \Delta\eta) = \left(\frac{C(\Delta\varphi, \Delta\eta)}{\langle C(\Delta\varphi, \Delta\eta) \rangle_{|\Delta\varphi|, |\Delta\eta| < 0.2}} \right)_{\text{Mixed Events}}.$$

Finally, the per-trigger azimuthal distribution $\tilde{C}_{\text{inclusive}}(\Delta\varphi)$ is obtained by integrating $\tilde{C}_{\text{inclusive}}(\Delta\varphi, \Delta\eta)$ in the range $|\Delta\eta| < 1$.

It was verified with Monte-Carlo simulations based on PYTHIA (Perugia-2011 tune) that the per-trigger azimuthal correlation of D mesons and secondary particles not rejected by the track selection has a $\Delta\varphi$ -dependent modulation with a maximum variation of 7% with respect to the azimuthal correlation of D mesons and primary particles. This $\Delta\varphi$ -dependent contamination has a negligible impact on the final results, considering the 4% level of contamination of secondary particles in the sample of associated tracks, hence, it was neglected.

A fraction of the reconstructed D mesons consists of secondary D mesons coming from B-meson decays. The topological cuts, applied to reject combinatorial background, select preferentially displaced vertices,

yielding a larger (by about a factor 2 for D^0 mesons in the measured p_T range) efficiency for secondary D mesons than for prompt D mesons. Therefore, the fraction f_{prompt} of reconstructed prompt D mesons does not coincide with the natural fraction and depends on the analysis details. The different fragmentation, as well as the contribution of B-meson decay particles and a possible different contribution of gluon splitting to charm- and beauty-quark production, imply a different angular-correlation distribution of prompt and secondary D mesons with charged particles, as it was verified with the Monte-Carlo simulations described in Section 2.2. The contribution of feed-down D mesons to the measured angular correlation is subtracted as follows:

$$\tilde{C}_{\text{prompt}}(\Delta\varphi) = \frac{1}{f_{\text{prompt}}} \left(\tilde{C}_{\text{inclusive}}(\Delta\varphi) - (1 - f_{\text{prompt}}) \tilde{C}_{\text{feed-down}}^{\text{MC templ}}(\Delta\varphi) \right). \quad (2)$$

In the above equation, $\tilde{C}_{\text{prompt}}(\Delta\varphi)$ is the per-trigger azimuthal-correlation distribution after the subtraction of the feed-down contribution, f_{prompt} is the fraction of prompt D mesons and $\tilde{C}_{\text{feed-down}}^{\text{MC templ}}(\Delta\varphi)$ is a template for the azimuthal-correlation distribution of the feed-down component. Using the same method described in [4], f_{prompt} was evaluated on the basis of FONLL calculations of charm and beauty p_T -differential production cross sections [1] and of the reconstruction efficiencies of prompt and secondary D mesons, calculated with Monte-Carlo simulations. The value of f_{prompt} , which depends on the D-meson species and varies as a function of p_T , is estimated to be larger than 75%. The azimuthal correlation of feed-down D mesons, $\tilde{C}_{\text{feed-down}}^{\text{MC templ}}$, was obtained from PYTHIA (tune Perugia 2011 [43]) simulations of pp collisions at $\sqrt{s} = 7$ TeV and $\sqrt{s} = 5.02$ TeV for the analysis of pp and p–Pb data, respectively. In order to avoid biases related to the different event multiplicity in real and simulated events, the correlation distribution was shifted to have its minimum coinciding with the baseline of the data azimuthal-correlation distribution before feed-down subtraction. A difference smaller than 8% was observed in the simulation between the baseline values of the azimuthal-correlation distributions for prompt and feed-down D mesons. Considering the typical values of f_{prompt} , this difference results in a shift of the baseline of $\tilde{C}_{\text{prompt}}(\Delta\varphi)$ smaller than 2%, negligible with respect to the other uncertainties affecting the measurement.

3.3 Characterization of azimuthal-correlation distributions

In order to quantify the properties of the measured azimuthal correlations, the following fit function is used:

$$f(\Delta\varphi) = b + \frac{A_{\text{NS}}}{\sqrt{2\pi}\sigma_{\text{fit,NS}}} e^{-\frac{(\Delta\varphi)^2}{2\sigma_{\text{fit,NS}}^2}} + \frac{A_{\text{AS}}}{\sqrt{2\pi}\sigma_{\text{fit,AS}}} e^{-\frac{(\Delta\varphi-\pi)^2}{2\sigma_{\text{fit,AS}}^2}}. \quad (3)$$

It is composed of two Gaussian terms describing the near- and away-side peaks and a constant term describing the baseline. A periodicity condition is also imposed to the function, requiring $f(0) = f(2\pi)$.

The integrals of the Gaussian terms, A_{NS} and A_{AS} , correspond to the associated-particle yields for the near (NS)- and away (AS)-side peaks, respectively, while $\sigma_{\text{fit,NS}}$ and $\sigma_{\text{fit,AS}}$ quantify the widths of the correlation peaks. By symmetry considerations, the mean of the Gaussian functions are fixed to $\Delta\varphi = 0$ and $\Delta\varphi = \pi$. The baseline b represents the physical minimum of the $\Delta\varphi$ distribution. To limit the effect of statistical fluctuations on the estimate of the associated yields, b is fixed to the weighted average of the points in the transverse region, defined as $\pi/4 < |\Delta\varphi| < \pi/2$, using the inverse of the square of the point statistical uncertainty as weights. Given the symmetry of the correlation distributions around $\Delta\varphi = 0$ and $\Delta\varphi = \pi$, the azimuthal distributions are reported in the range $0 < \Delta\varphi < \pi$ to reduce statistical fluctuations.

4 Systematic uncertainties

The fit of the D-meson invariant-mass distribution introduces systematic uncertainties on S_{peak} and B_{peak} (Section 3.1, Equation 1). The uncertainty on the correlation distribution was estimated by calculating

B_{peak} from the integral of the background term of the invariant-mass fit function in the range $|M - \mu| < 2\sigma$ and by varying the fit procedure. In particular, the fit was repeated modeling the background distribution with a linear function and a parabola instead of an exponential function (for D^0 and D^+ mesons only), considering a different histogram binning, and varying the fit range. A 10% systematic uncertainty was estimated from the corresponding variation of the azimuthal-correlation distribution. No significant trend was observed as a function of $\Delta\phi$ and the same uncertainty was estimated for all D-meson species in all p_T -intervals and in both pp and p–Pb collision systems.

A 5% uncertainty (10% for D^+ mesons in p–Pb collisions) derives from the possible dependence of the shape of $\tilde{C}(\Delta\phi, \Delta\eta)_{\text{sidebands}}$ on the sideband range. This source of uncertainty was determined by restricting the invariant-mass sideband window to the intervals $4\sigma < |M - \mu| < 6\sigma$ or to $6\sigma < |M - \mu| < 8\sigma$ for all the D mesons, and also by considering, for D^0 and D^+ mesons, only the left or only the right sideband.

The uncertainty on the correction for the associated-particle reconstruction efficiency was assessed by varying the selection criteria applied to the reconstructed tracks, removing the request of at least three associated clusters in the ITS, or demanding a hit on at least one of the two SPD layers. A $\pm 4\%$ uncertainty was estimated for p–Pb collisions, while a $^{+10\%}_{-5\%}$ contribution was obtained for the pp analysis, with the +10% contribution arising from the request of hits in the SPD. No significant trend in $\Delta\phi$ was observed.

The uncertainty on the residual contamination from secondary tracks was evaluated by repeating the analysis varying the cut on the DCA in the (x, y) plane from 0.1 cm to 1 cm, and re-evaluating the purity of charged primary particles for each variation. This resulted in a 5% (3.5%) systematic uncertainty in pp (p–Pb) collisions, independent of $\Delta\phi$ and p_T^{assoc} .

A 5% systematic effect originating from the correction of the D-meson reconstruction efficiency was evaluated by applying a tighter and a looser topological selection on the D-meson candidates. No significant dependence on $\Delta\phi$ was observed and the same uncertainty was estimated for the three D-meson p_T intervals, apart from D^+ meson in p–Pb collisions, for which a 10% uncertainty was assigned.

The uncertainty on the subtraction of the beauty feed-down contribution was quantified by generating the templates of feed-down azimuthal-correlation distributions, $\tilde{C}_{\text{feed-down}}^{\text{MC templ}}(\Delta\phi)$ in Equation 2, with different PYTHIA 6 tunes (Perugia 0, Perugia 2010, see Section 2.2), and by considering the range of f_{prompt} values obtained by varying the prompt and feed-down D-meson p_T -differential production cross sections within FONLL uncertainty band, as described in [4]. The effect on the azimuthal-correlation distributions is $\Delta\phi$ dependent and contained within 8% and is more pronounced in the near side, in particular in the lowest and middle D-meson p_T intervals.

The consistency of the whole correction procedure, prior to the feed-down subtraction, was verified by performing the analysis of simulated events (“Monte Carlo closure test”) separately for prompt and feed-down D mesons. For prompt D mesons, no effect was found for both pp and p–Pb collision systems. Conversely, for feed-down D mesons, an overestimate by about 20% in the near side was found for both collision systems. It was verified that the source of this excess is related to a bias induced by the topological selection applied to D mesons, that tends to favour cases with a small angular opening between the products of the beauty-hadron decay, thus between the D meson and the other decay particles. This effect results in a $\Delta\phi$ -dependent overestimate of the feed-down subtracted correlation distribution in the near side, contained within 2%.

The systematic uncertainties affecting the $\Delta\phi$ -correlation distributions are summarized in Table 1 for both pp and p–Pb collision systems. The $\Delta\phi$ -dependent parts of the uncertainties arising from the feed-down subtraction and the Monte-Carlo closure test define the $\Delta\phi$ -uncorrelated systematic uncertainties. All the other contributions, correlated in $\Delta\phi$, act as a scale uncertainty. No significant dependence on

the transverse momentum of D mesons and associated particles was observed for both $\Delta\phi$ -correlated and uncorrelated uncertainties, except for the feed-down systematic uncertainty.

System	pp	p–Pb
D-meson species	D^0, D^{*+}, D^+	$D^0, D^{*+} (D^+)$
Signal, background normalization	$\pm 10\%$	$\pm 10\%$
Background $\Delta\phi$ distribution	$\pm 5\%$	$\pm 5\% (\pm 10\%)$
Associated-track reconstruction efficiency	$+10\%, -5\%$	$\pm 4\%$
Primary-particle purity	$\pm 5\%$	$\pm 3.5\%$
D-meson efficiency	$\pm 5\%$	$\pm 5\% (\pm 10\%)$
Feed-down subtraction	up to 8%, $\Delta\phi$ dependent	up to 8%, $\Delta\phi$ dependent
MC closure test	-2% (near side)	-2% (near side), $\pm 2\%$

Table 1: List of systematic uncertainties for the $\Delta\phi$ -correlation distributions in pp and p–Pb collisions. See text for details.

Different approaches were applied to estimate the systematic uncertainty on the near-side peak associated yield and peak width and on the baseline, obtained from the A_{NS} , $\sigma_{fit,NS}$, and b parameters of the fit of the azimuthal-correlation distribution, as described in Section 3.3. The main source of uncertainty derives from the definition of the baseline itself, which is connected to the assumption that the observed variation of the azimuthal-correlation distribution in the transverse region is determined mainly by statistical fluctuations rather than by the true physical trend. The variation of A_{NS} , $\sigma_{fit,NS}$, and b values obtained when considering a $\pm\pi/4$ variation of the $\Delta\phi$ range defining the transverse region is interpreted as the systematic uncertainty due to the baseline definition. In addition, the fits were repeated by moving upwards and downwards the data points by the corresponding value of the $\Delta\phi$ -uncorrelated systematic uncertainty. The final systematic uncertainty was calculated by summing in quadrature the aforementioned contributions and, for the associated yields and baseline, also the systematic uncertainty correlated in $\Delta\phi$. The values of the total systematic uncertainties on the near-side peak yield, width, and baseline are reported in Table 2, for two intervals of transverse momentum of D mesons and associated particles. Considering all the measured kinematic ranges, the uncertainties vary from $\pm 12\%$ to $\pm 25\%$ for the near-side peak yield, from $\pm 2\%$ to $\pm 13\%$ for the near-side peak width and from $\pm 11\%$ to $\pm 16\%$ for the baseline. Typically, lower uncertainties are obtained for p–Pb collisions, where the larger available statistics of the correlation distributions allows for a more precise estimate of the baseline height, which constitutes the main source of uncertainty also on the evaluation of the near-side peak associated yield and width.

System	pp		p–Pb	
	$5 < p_T^D < 8 \text{ GeV}/c,$ $0.3 < p_T^{\text{assoc}} < 1 \text{ GeV}/c$	$8 < p_T^D < 16 \text{ GeV}/c,$ $p_T^{\text{assoc}} > 1 \text{ GeV}/c$	$5 < p_T^D < 8 \text{ GeV}/c,$ $0.3 < p_T^{\text{assoc}} < 1 \text{ GeV}/c$	$8 < p_T^D < 16 \text{ GeV}/c,$ $p_T^{\text{assoc}} > 1 \text{ GeV}/c$
NS yield	$\pm 22\%$	$\pm 15\%$	$\pm 17\%$	$\pm 12\%$
NS width	$\pm 10\%$	$\pm 5\%$	$\pm 3\%$	$\pm 3\%$
Baseline	$\pm 13\%$	$\pm 15\%$	$\pm 12\%$	$\pm 11\%$

Table 2: List of systematic uncertainties for near-side (NS) peak associated yield, near-side peak width, and baseline in pp and p–Pb collisions, for two different kinematic ranges of D mesons and associated particles. See text for details.

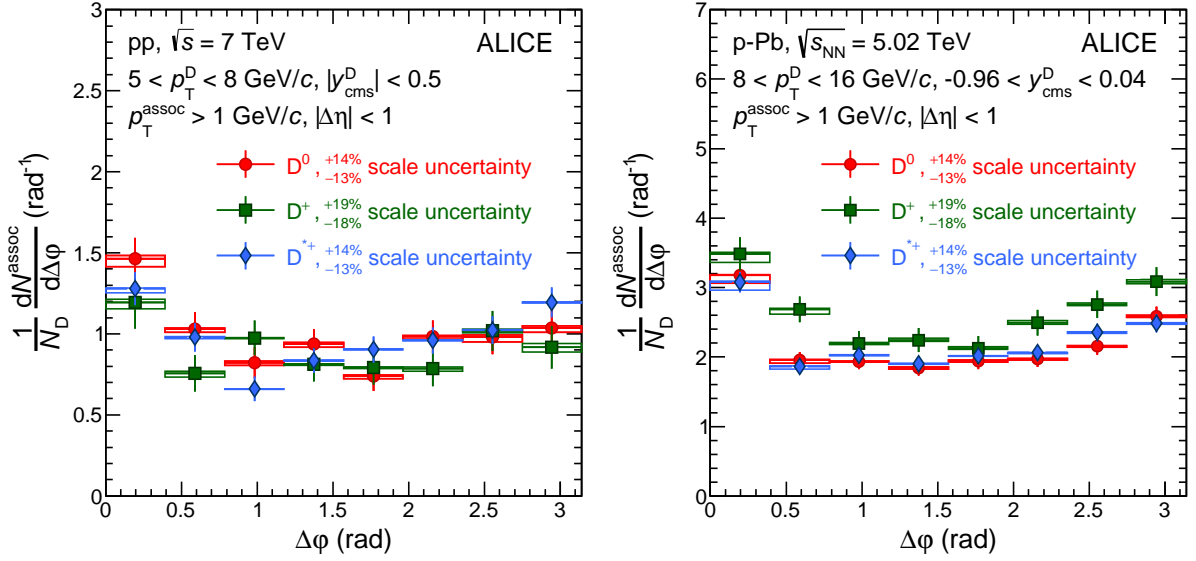


Figure 1: Comparison of the azimuthal-correlation distributions of D mesons and charged particles obtained for D^0 , D^+ and D^{*+} mesons for $5 < p_T^D < 8$ GeV/c, $p_T^{\text{assoc}} > 1$ GeV/c in pp collisions at $\sqrt{s} = 7$ TeV (left panel) and for $8 < p_T^D < 16$ GeV/c, $p_T^{\text{assoc}} > 1$ GeV/c in p–Pb collisions at $\sqrt{s_{\text{NN}}} = 5.02$ TeV (right panel). The statistical uncertainties are shown as error bars, the $\Delta\phi$ -uncorrelated systematic uncertainties as boxes, while the part of systematic uncertainty correlated in $\Delta\phi$ is reported as text (scale uncertainty). The latter is largely uncorrelated among the D-meson species.

5 Results

The azimuthal-correlation distributions of D^0 , D^+ , D^{*+} mesons and charged particles with $p_T^{\text{assoc}} > 1$ GeV/c are compared in Figure 1 for $5 < p_T^D < 8$ GeV/c in pp collisions (left panel) and for $8 < p_T^D < 16$ GeV/c in p–Pb collisions (right panel). The distributions obtained with the three D-meson species are compatible within the quadratic sum (w_i , $i = D^0, D^+, D^{*+}$) of the statistical uncertainty and of the systematic uncertainties on the signal, background normalization, and on the background shape (see Table 1), that are uncorrelated among the three meson species. The D^0 -, D^+ -, D^{*+} -meson data are averaged using $1/w_i^2$ as weights. The averages of the distributions are shown, for all the considered kinematic ranges, in Figure 2 for pp and p–Pb collisions. As expected, a rising trend of the height of the near-side peak with increasing D-meson p_T is observed for both collision systems, together with a decrease of the baseline level with increasing p_T of the associated particles.

Figure 3 shows the $\Delta\phi$ distributions after the subtraction of the baseline, calculated as described in Section 3.3. The distributions show a near-side peak and a wider and lower peak in the away-side region. The results obtained for the two collision systems are compatible within uncertainties. According to simulations of pp collisions performed with PYTHIA 6 (Perugia-0, -2010, and -2011 tunes), the different centre-of-mass energy and the slightly different D-meson rapidity range of the two measurements should induce variations in the baseline-subtracted azimuthal-correlation distributions smaller than 7% in the near- and away-side regions. The same estimate is obtained with POWHEG+PYTHIA simulations including the EPS09 parametrization of nuclear PDFs (see Section 2.2). Such differences are well below the current level of uncertainties.

A further comparison of pp and p–Pb collision results has been done by quantifying the integrals and the widths of the near-side correlation peaks by fitting the measured distributions as described in Section 3.3. The fit results are reported only for the near-side peak parameters and the baseline because of the poor statistical precision on the fit parameters of the away-side peaks. Figure 4 shows, as an example, the fit to the azimuthal-correlation distributions of D mesons and charged particles with

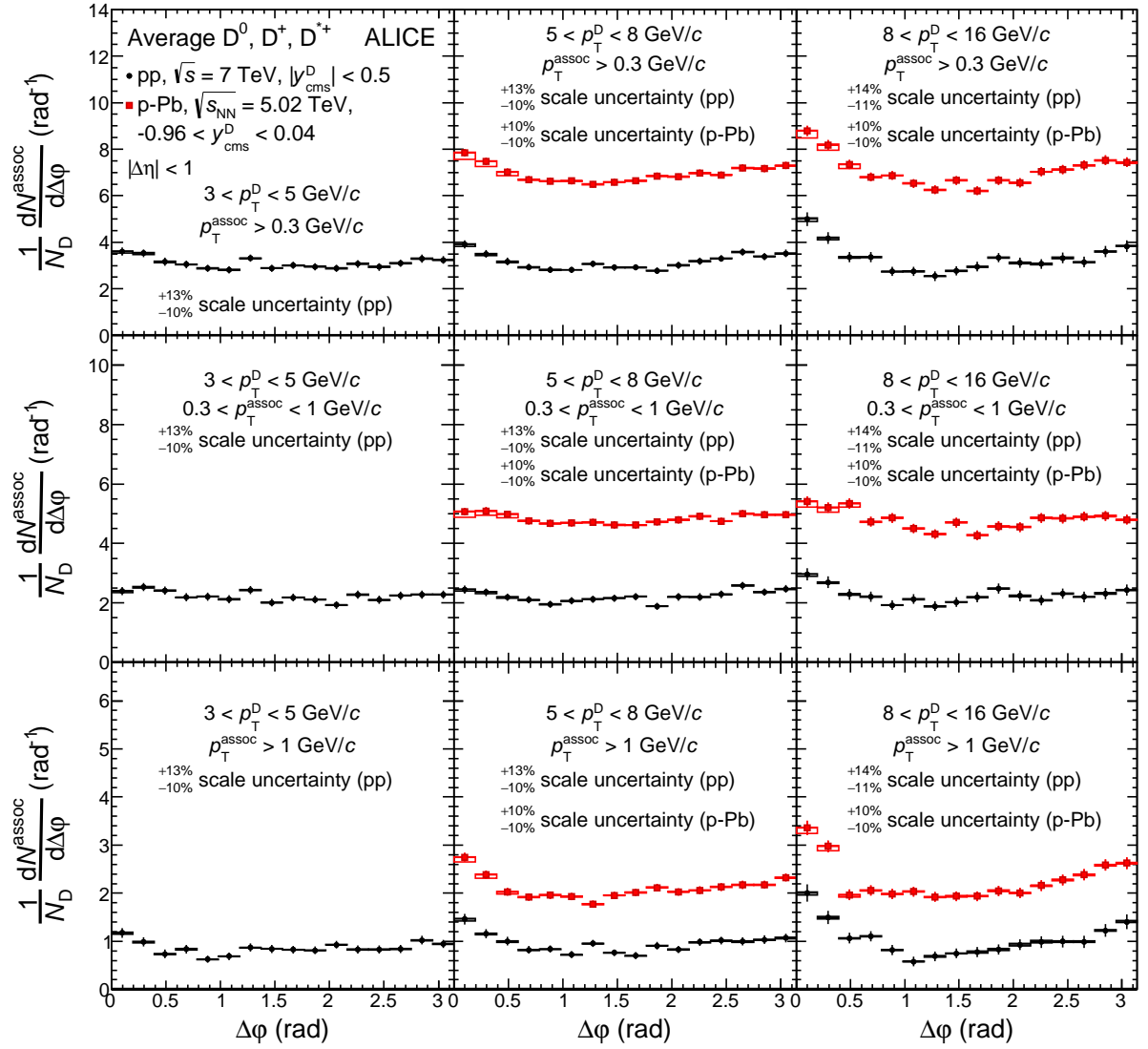


Figure 2: Average of the azimuthal-correlation distributions of D^0 , D^+ and D^{*+} mesons with $3 < p_T^D < 5$ GeV/ c (left column), $5 < p_T^D < 8$ GeV/ c (middle column), and $8 < p_T^D < 16$ GeV/ c (right column) and charged particles with $p_T^{\text{assoc}} > 0.3$ GeV/ c (top row), $0.3 < p_T^{\text{assoc}} < 1$ GeV/ c (middle row), and $p_T^{\text{assoc}} > 1$ GeV/ c (bottom row), measured in pp collisions at $\sqrt{s} = 7$ TeV and in p–Pb collisions at $\sqrt{s_{\text{NN}}} = 5.02$ TeV. The statistical uncertainties are shown as error bars, the $\Delta\phi$ -uncorrelated systematic uncertainties as boxes, while the part of systematic uncertainty correlated in $\Delta\phi$ is reported as text (scale uncertainty).

$p_T^{\text{assoc}} > 1$ GeV/ c , for $5 < p_T^D < 8$ GeV/ c in pp collisions (left panel) and for $8 < p_T^D < 16$ GeV/ c in p–Pb collisions (right panel). The curves superimposed to the data represent the three terms of the function defined in Equation 3. The fit function describes, within uncertainties, the measured distributions in all kinematic cases considered, providing values of χ^2/NDF close to unity. The evolution of the near-side peak associated yield as a function of the D-meson p_T is reported in Figure 5 (top row), for pp and p–Pb collisions, for $p_T^{\text{assoc}} > 0.3$ GeV/ c (left panel) and for the two sub-intervals $0.3 < p_T^{\text{assoc}} < 1$ GeV/ c (middle panel) and $p_T^{\text{assoc}} > 1$ GeV/ c (right panel). The near-side peak associated yield exhibits an increasing trend with D-meson p_T and has similar values, within uncertainties, for the softer ($0.3 < p_T^{\text{assoc}} < 1$ GeV/ c) and the harder ($p_T^{\text{assoc}} > 1$ GeV/ c) sub-ranges of p_T^{assoc} used, in each D-meson p_T interval considered. The values obtained for pp and p–Pb collision data are compatible within statistical uncertainties. In the bottom row of the same figure the width of the near-side Gaussian

term ($\sigma_{\text{fit,NS}}$) is shown. Although the case with $p_{\text{T}}^{\text{assoc}} > 0.3$ GeV/ c seems to suggest that $\sigma_{\text{fit,NS}}$ does not strongly depend on D-meson p_{T} in the range of the measurement, the current level of uncertainty does not allow to quantify the dependence of $\sigma_{\text{fit,NS}}$ on D-meson and associated charged particle p_{T} , as well as a possible difference between the values measured for pp and p–Pb collisions. In particular, our approach for the calculation of the baseline (Section 3.3) guarantees a robust estimate of the minimum, but the baseline uncertainty and its impact on the associated-yield uncertainty are rather large (Section 4). This systematic uncertainty is expected to be significantly reduced in future measurements with larger data samples, where a smaller $\Delta\phi$ range for the baseline calculation could be used.

A v_2 -like modulation of the baseline would introduce a bias in the measurement of the associated yield and peak width that needs to be taken into account while interpreting the measured quantities in terms of charm-jet properties. In order to get an estimate of this possible effect, for the p–Pb case the fit was repeated by subtracting from the correlation distribution a v_2 -like modulation assuming $v_2 = 0.05$ for D mesons and $v_2 = 0.05$ (0.1) for associated charged particles with $p_{\text{T}} > 0.3$ (1) GeV/ c . These values were chosen on the basis of charged-particle measurements in high-multiplicity p–Pb collisions [20] and assuming for D mesons the maximum value predicted in [37] for the 20% most central p–Pb collisions as a test case. With such assumptions, rather extreme also considering that this measurement is performed without any selection on event multiplicity, A_{NS} varies by -10% (-6%) for D mesons with $5 < p_{\text{T}} < 8$ GeV/ c and for $0.3 < p_{\text{T}}^{\text{assoc}} < 1$ GeV/ c ($p_{\text{T}}^{\text{assoc}} > 1$ GeV/ c). The variations on $\sigma_{\text{fit,NS}}$ and on the baseline are below 4% and 1%, respectively. Significantly smaller modifications result for D mesons with $8 < p_{\text{T}} < 16$ GeV/ c . With the available statistics, the precision of the measurement is not sufficient to observe or exclude these modifications.

Figure 6 shows the comparison of the averaged azimuthal-correlation distributions measured in pp collisions with expectations from simulations performed with PYTHIA and POWHEG+PYTHIA (see Section 2.2), after the baseline subtraction. In the case of the simulations, for which statistical fluctuations are negligible, the baseline is estimated as the minimum of the azimuthal-correlation distribution. The average of the two lowest values is used to define the uncertainty related to the baseline definition in Monte-Carlo simulations. This uncertainty is negligible and not displayed in the figures. The distributions obtained with the different generators and tunes do not show significant differences in the near side. In the away side, the PYTHIA 6 tunes Perugia 0 and Perugia 2010 tend to have higher correlation values, especially for $p_{\text{T}}^{\text{assoc}} > 1$ GeV/ c , compared to the other simulation results. All the considered Monte-Carlo simulations describe, within the uncertainties, the data in the whole $\Delta\phi$ range, though a hint for a more pronounced peak in the near side in data than in models is present for D mesons with $8 < p_{\text{T}} < 16$ GeV/ c for $p_{\text{T}}^{\text{assoc}} > 0.3$ GeV/ c . This can also be observed from the comparison of the associated yield in the near-side peak in data and in simulations, displayed in the top row of Figures 7 and 8, for pp and p–Pb collisions, respectively. For both collision systems the measured associated yield is larger by a factor about 1.5 with respect to PYTHIA 8 and POWHEG+PYTHIA predictions for D mesons with $8 < p_{\text{T}} < 16$ GeV/ c and $p_{\text{T}}^{\text{assoc}} > 0.3$ GeV/ c , though still compatible within less than 2σ . The width of the near-side peaks, shown in the second row of the same figures, seems to be better reproduced by the simulations in the case of p–Pb than of pp results. The evolution of the baseline value as a function of the D-meson p_{T} is compared for pp-collision data to expectations from PYTHIA simulations in the bottom row of Figure 7 for the three ranges of $p_{\text{T}}^{\text{assoc}}$ considered in the analysis. The value of the baseline, mainly determined by the event multiplicity, does not show substantial variations as a function of D-meson p_{T} , as expected also from PYTHIA simulations, which reproduce the observed values within the uncertainties.

6 Summary

The first measurements of the azimuthal correlations between D mesons and charged particles in pp and p–Pb collisions at $\sqrt{s} = 7$ TeV and $\sqrt{s_{\text{NN}}} = 5.02$ TeV, respectively, performed with the ALICE detector at

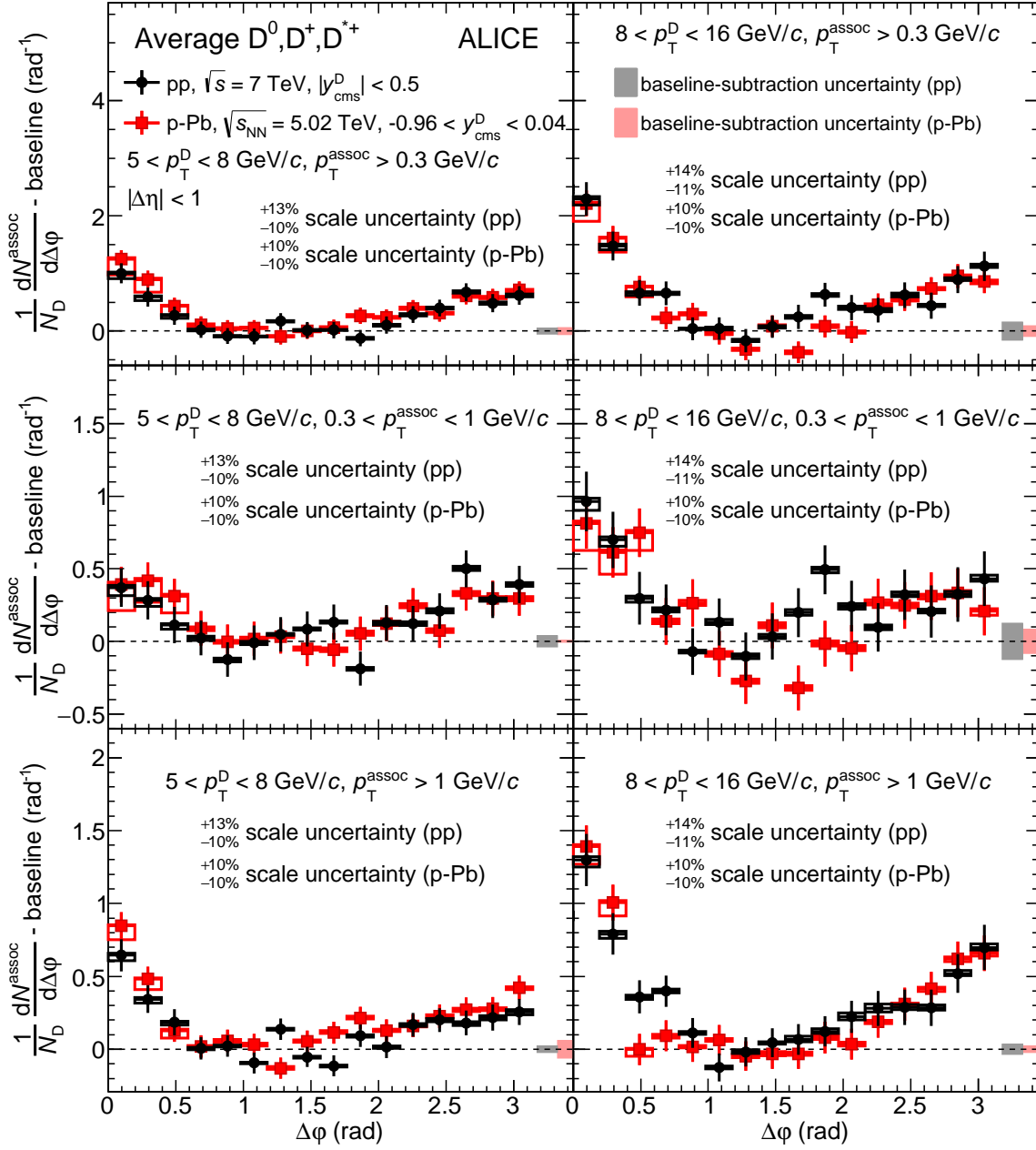


Figure 3: Comparison of the azimuthal-correlation distributions of D mesons with $5 < p_T^D < 8$ GeV/c (left column) and $8 < p_T^D < 16$ GeV/c (right column) and charged particles with $p_T^{\text{assoc}} > 0.3$ GeV/c (top row), $0.3 < p_T^{\text{assoc}} < 1$ GeV/c (middle row), and $p_T^{\text{assoc}} > 1$ GeV/c (bottom row) in pp collisions at $\sqrt{s} = 7$ TeV and in p-Pb collisions at $\sqrt{s_{\text{NN}}} = 5.02$ TeV, after subtracting the baseline. The statistical uncertainties are shown as error bars, the $\Delta\phi$ -uncorrelated systematic uncertainties as boxes around the data points, the part of systematic uncertainty correlated in $\Delta\phi$ is reported as text (scale uncertainty), the uncertainties deriving from the subtraction of the baselines are represented by the boxes at $\Delta\phi > \pi$.

the LHC, were presented. The $\Delta\phi$ distributions were studied in pp collisions in three different D-meson transverse-momentum intervals, $3 < p_T^D < 5$ GeV/c, $5 < p_T^D < 8$ GeV/c, and $8 < p_T^D < 16$ GeV/c, for associated charged particles with $p_T^{\text{assoc}} > 0.3$ GeV/c, and in the two sub-ranges $0.3 < p_T^{\text{assoc}} < 1$ GeV/c and $p_T^{\text{assoc}} > 1$ GeV/c. For p-Pb collisions, the results were reported in two D-meson p_T ranges,

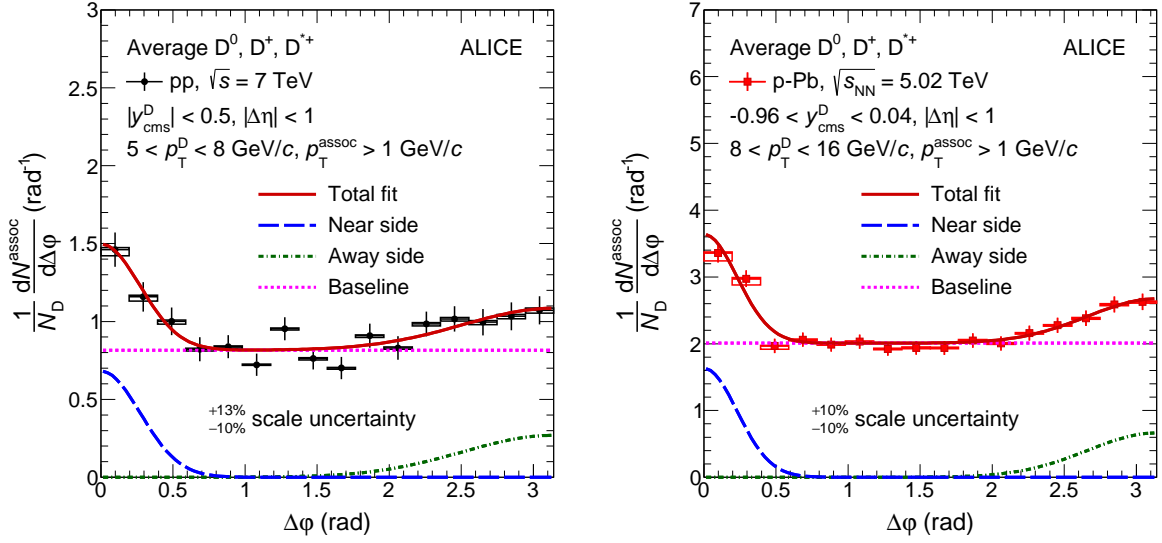


Figure 4: Examples of the fit to the azimuthal-correlation distribution, for D mesons with $5 < p_T^D < 8$ GeV/c and charged particles with $p_T^{\text{assoc}} > 1$ GeV/c in pp collisions at $\sqrt{s} = 7$ TeV (left), and for D mesons with $8 < p_T^D < 16$ GeV/c and charged particles with $p_T^{\text{assoc}} > 1$ GeV/c in p-Pb collisions at $\sqrt{s_{\text{NN}}} = 5.02$ TeV (right). The statistical uncertainties are shown as error bars, the $\Delta\phi$ -uncorrelated systematic uncertainties as boxes, while the part of systematic uncertainty correlated in $\Delta\phi$ is reported as text (scale uncertainty). The terms of the fit function described in Section 3.3 are also shown separately: near-side Gaussian function (blue dashed line), away-side Gaussian function (green dashed-dotted line) and baseline constant term (magenta dotted line).

$5 < p_T^D < 8$ GeV/c, and $8 < p_T^D < 16$ GeV/c. The baseline-subtracted azimuthal-correlation distributions observed in the two collision systems are compatible within uncertainties. The variations expected from the lower nucleon-nucleon centre-of-mass energy of p-Pb collisions and from the slightly different D-meson rapidity ranges used for the p-Pb analysis were studied with simulated pp collisions at the two centre-of-mass energies and are well below the sensitivity of the measurements.

The properties of the near-side correlation peak, sensitive to the characteristics of the jet containing the D meson, were described in terms of the yield of associated charged particles and peak width, obtained by fitting the $\Delta\phi$ distributions with a function composed of a constant term, representing the physical minimum of the distribution, and two Gaussian terms modeling the near- and away-side peaks. The values measured in the two collision systems are compatible within uncertainties.

The measured azimuthal distributions, as well as the properties of the correlation peaks, were compared to expectations from simulations performed with different Monte-Carlo generators. The simulations reproduce the correlation distributions within uncertainties.

Considering that the overall uncertainty is dominated by the statistical component, the data collected from pp collisions at $\sqrt{s} = 13$ TeV in the ongoing Run 2 at the LHC will allow for a more precise measurement. In particular, the predicted increase of the cross section for charm production by more than a factor 2 at $p_T = 10$ GeV/c at the higher collision energy [1], along with the foreseen larger integrated luminosity, will allow for a significant reduction of the statistical uncertainty, providing a more quantitative and constraining comparison of the data with expectations from Monte-Carlo generators. As mentioned in Section 5, with larger data samples a different determination of the baseline of the azimuthal-correlation distribution will become possible, bringing to a significant reduction of the systematic uncertainty on the measurement of the associated yields. The data that will be collected in next p-Pb collision runs at the LHC may also allow a study of the evolution of the azimuthal-correlation distribution as a function of the event multiplicity, searching for possible long-range ridge-like structures already observed with correlation of light particles.

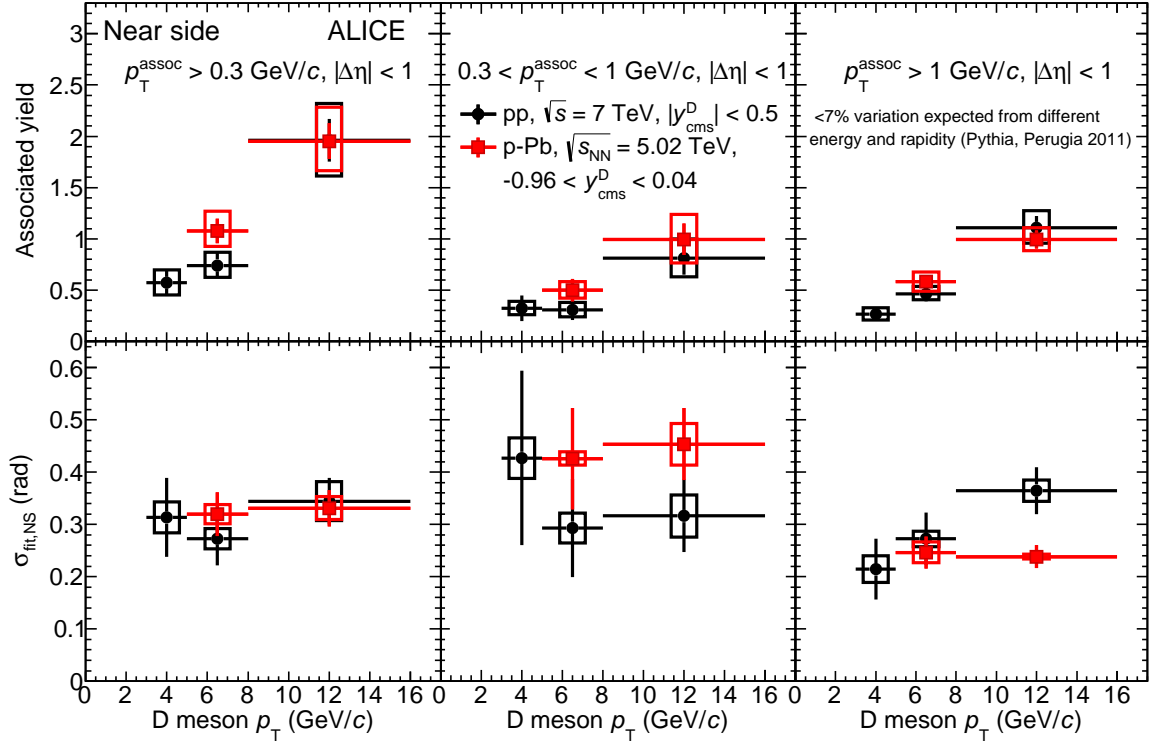


Figure 5: Comparison of the near-side peak associated yield (top row) and peak width (bottom row) in pp and p–Pb collisions as a function of p_T^D , for $p_T^{\text{assoc}} > 0.3$ GeV/ c (left column), $0.3 < p_T^{\text{assoc}} < 1$ GeV/ c (middle column), and $p_T^{\text{assoc}} > 1$ GeV/ c (right column). Statistical and systematic uncertainties are shown as error bars and boxes, respectively.

The results reported in this paper represent a first step towards the measurement of possible modifications of the azimuthal correlation of D mesons and charged particles in Pb–Pb collisions, that could provide important information on the charm-quark energy-loss mechanisms in the presence of the medium formed in heavy-ion collisions at LHC energies. Given the same collision energy, the p–Pb results presented in this paper could serve as a reference to study medium effects in Pb–Pb collisions at $\sqrt{s_{\text{NN}}} = 5.02$ TeV collected in the LHC Run 2.

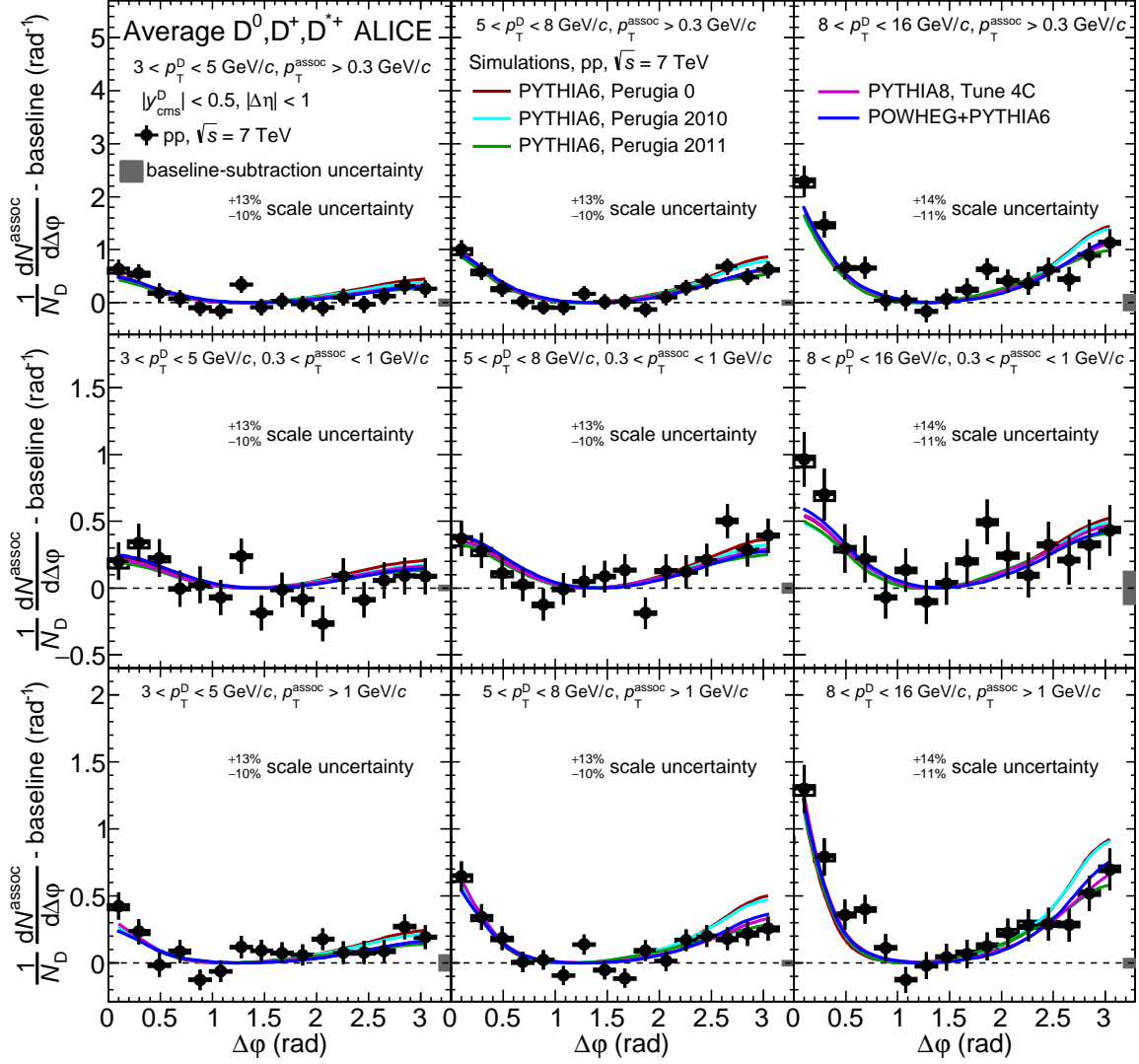


Figure 6: Comparison of $\Delta\phi$ -correlation distributions of D mesons and charged particles measured in pp collisions at $\sqrt{s} = 7$ TeV and Monte-Carlo simulations performed with different event generators, after the subtraction of the baseline. The statistical and systematic uncertainties of the measured distributions are displayed as in Figure 3.

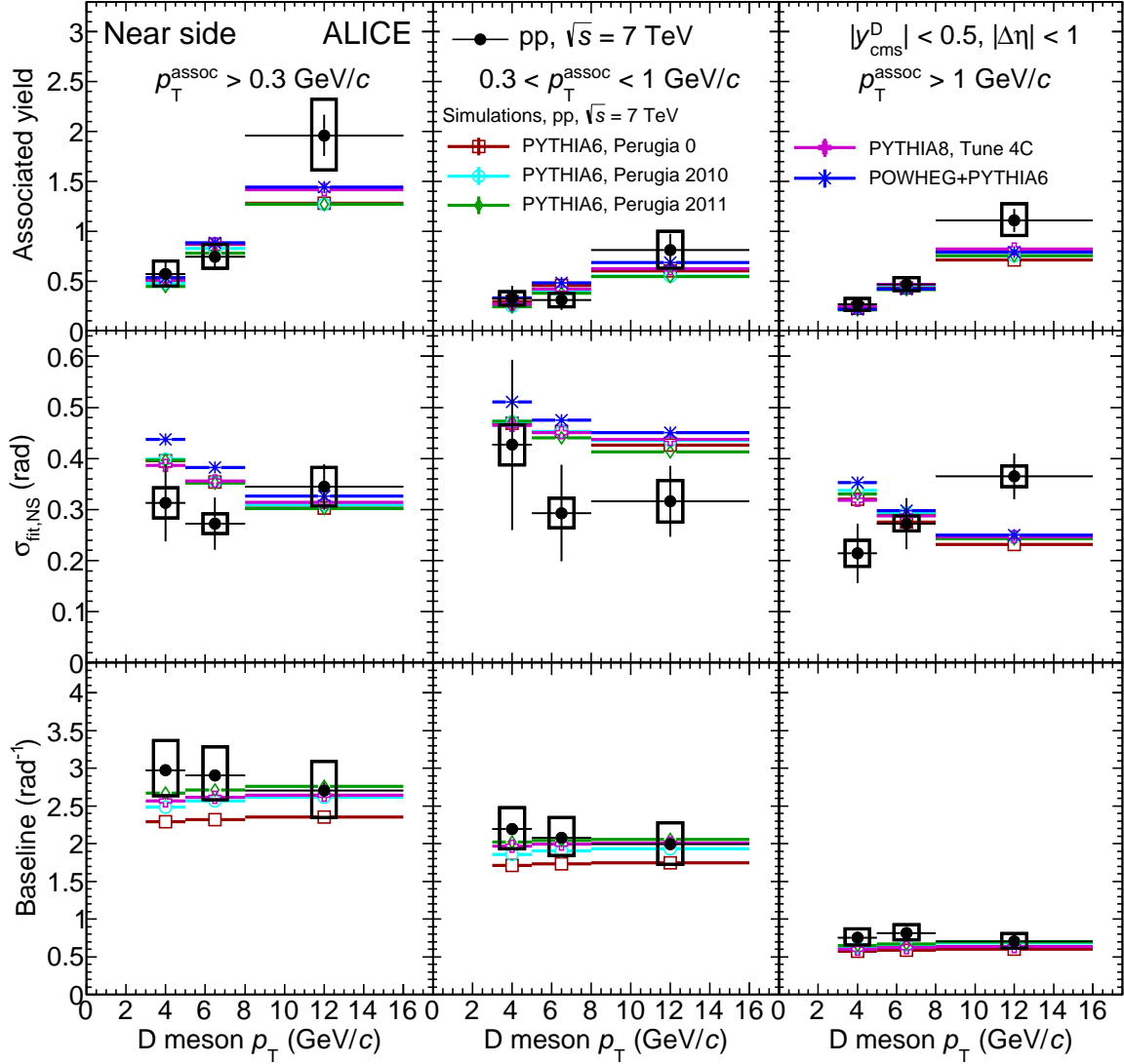


Figure 7: Comparison of near-side peak associated yield (top row), near-side peak width (middle row), and baseline (bottom row) values measured in pp collisions at $\sqrt{s} = 7$ TeV with the expectations from simulations performed with different Monte-Carlo event generators. Statistical and systematic uncertainties are shown as error bars and boxes, respectively.

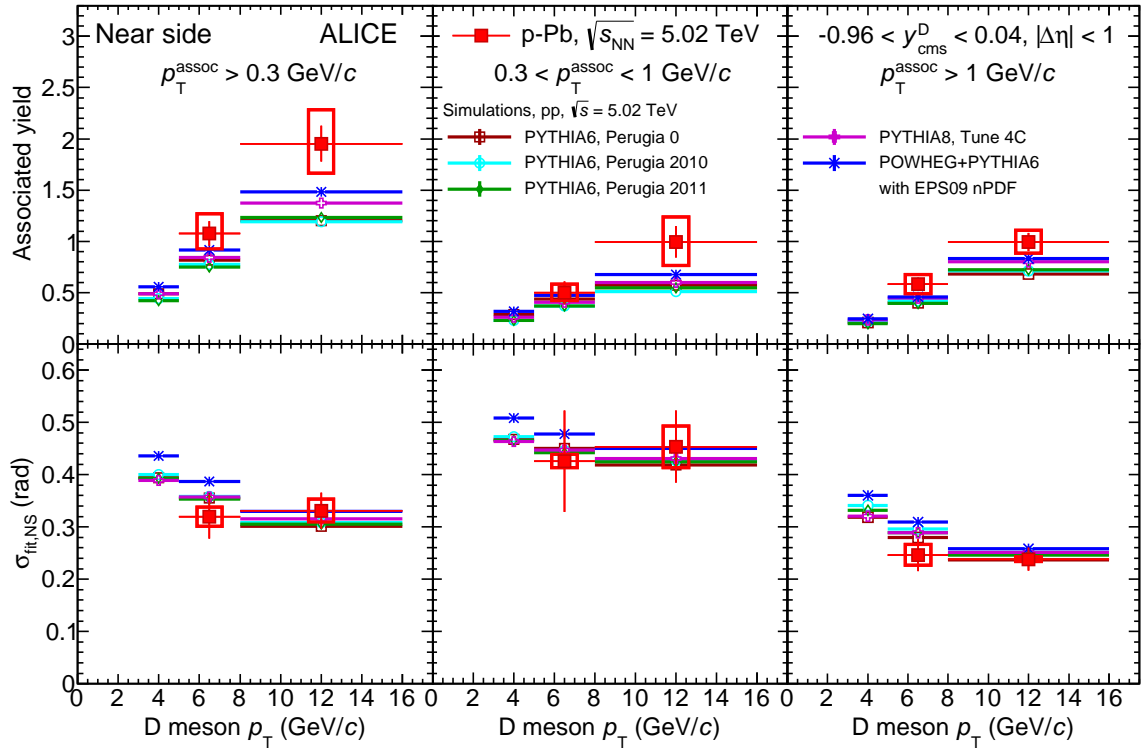


Figure 8: Comparison of near-side peak associated yield (top row) and near-side peak width (bottom row) values measured in p–Pb collisions at $\sqrt{s_{NN}} = 5.02$ TeV with the expectations from simulations performed with different Monte-Carlo event generators. Statistical and systematic uncertainties are shown as error bars and boxes, respectively.

Acknowledgements

The ALICE Collaboration would like to thank all its engineers and technicians for their invaluable contributions to the construction of the experiment and the CERN accelerator teams for the outstanding performance of the LHC complex. The ALICE Collaboration gratefully acknowledges the resources and support provided by all Grid centres and the Worldwide LHC Computing Grid (WLCG) collaboration. The ALICE Collaboration acknowledges the following funding agencies for their support in building and running the ALICE detector: State Committee of Science, World Federation of Scientists (WFS) and Swiss Fonds Kidagan, Armenia; Conselho Nacional de Desenvolvimento Científico e Tecnológico (CNPq), Financiadora de Estudos e Projetos (FINEP), Fundação de Amparo à Pesquisa do Estado de São Paulo (FAPESP); Ministry of Science & Technology of China (MSTC), National Natural Science Foundation of China (NSFC) and Ministry of Education of China (MOEC); Ministry of Science, Education and Sports of Croatia and Unity through Knowledge Fund, Croatia; Ministry of Education and Youth of the Czech Republic; Danish Natural Science Research Council, the Carlsberg Foundation and the Danish National Research Foundation; The European Research Council under the European Community’s Seventh Framework Programme; Helsinki Institute of Physics and the Academy of Finland; French CNRS-IN2P3, the ‘Region Pays de Loire’, ‘Region Alsace’, ‘Region Auvergne’ and CEA, France; German Bundesministerium für Bildung, Wissenschaft, Forschung und Technologie (BMBF) and the Helmholtz Association; General Secretariat for Research and Technology, Ministry of Development, Greece; National Research, Development and Innovation Office (NKFIH), Hungary; Council of Scientific and Industrial Research (CSIR), New Delhi; Department of Atomic Energy and Department of Science and Technology of the Government of India; Istituto Nazionale di Fisica Nucleare (INFN) and Centro Fermi - Museo Storico della Fisica e Centro Studi e Ricerche “Enrico Fermi”, Italy; Japan Society for the Promotion of Science (JSPS) KAKENHI and MEXT, Japan; National Research Foundation of Korea (NRF); Consejo Nacional de Ciencia y Tecnología (CONACYT), Dirección General de Asuntos del Personal Académico (DGAPA), México, Amérique Latine Formation académique - European Commission (ALFA-EC) and the EPLANET Program (European Particle Physics Latin American Network); Stichting voor Fundamenteel Onderzoek der Materie (FOM) and the Nederlandse Organisatie voor Wetenschappelijk Onderzoek (NWO), Netherlands; Research Council of Norway (NFR); Pontificia Universidad Católica del Perú; National Science Centre, Poland; Ministry of National Education/Institute for Atomic Physics and National Council of Scientific Research in Higher Education (CNCSI-UEFISCDI), Romania; Joint Institute for Nuclear Research, Dubna; Ministry of Education and Science of Russian Federation, Russian Academy of Sciences, Russian Federal Agency of Atomic Energy, Russian Federal Agency for Science and Innovations and The Russian Foundation for Basic Research; Ministry of Education of Slovakia; Department of Science and Technology, South Africa; Centro de Investigaciones Energéticas, Medioambientales y Tecnológicas (CIEMAT), E-Infrastructure shared between Europe and Latin America (EELA), Ministerio de Economía y Competitividad (MINECO) of Spain, Xunta de Galicia (Consellería de Educación), Centro de Aplicaciones Tecnológicas y Desarrollo Nuclear (CEADEN), Cubaenergía, Cuba, and IAEA (International Atomic Energy Agency); Swedish Research Council (VR) and Knut & Alice Wallenberg Foundation (KAW); National Science and Technology Development Agency (NSDTA), Suranaree University of Technology (SUT) and Office of the Higher Education Commission under NRU project of Thailand; Ukraine Ministry of Education and Science; United Kingdom Science and Technology Facilities Council (STFC); The United States Department of Energy, the United States National Science Foundation, the State of Texas, and the State of Ohio.

References

- [1] M. Cacciari, M. Greco, and P. Nason, “The p_T spectrum in heavy flavor hadroproduction,” *JHEP* **05** (1998) 007, arXiv:hep-ph/9803400 [hep-ph].

- [2] B. A. Kniehl, G. Kramer, I. Schienbein, and H. Spiesberger, “Inclusive Charmed-Meson Production at the CERN LHC,” *Eur. Phys. J.* **C72** (2012) 2082, arXiv:1202.0439 [hep-ph].
- [3] R. Maciula and A. Szczurek, “Open charm production at the LHC - k_T -factorization approach,” *Phys. Rev.* **D87** (2013) 094022, arXiv:1301.3033 [hep-ph].
- [4] ALICE Collaboration, B. Abelev *et al.*, “Measurement of charm production at central rapidity in proton-proton collisions at $\sqrt{s} = 7$ TeV,” *JHEP* **01** (2012) 128, arXiv:1111.1553 [hep-ex].
- [5] ALICE Collaboration, B. Abelev *et al.*, “Measurement of charm production at central rapidity in proton-proton collisions at $\sqrt{s} = 2.76$ TeV,” *JHEP* **07** (2012) 191, arXiv:1205.4007 [hep-ex].
- [6] T. Sjostrand, S. Mrenna, and P. Z. Skands, “PYTHIA 6.4 Physics and Manual,” *JHEP* **05** (2006) 026, arXiv:hep-ph/0603175 [hep-ph].
- [7] G. Corcella, I.G. Knowles, G. Marchesini, S. Moretti, K. Odagiri, P. Richardson, M.H. Seymour, and B.R. Webber, “HERWIG 6: an event generator for hadron emission reactions with interfering gluons (including supersymmetric processes),” *JHEP* **0101** (2001) 010.
- [8] M. L. Mangano, P. Nason, and G. Ridolfi, “Heavy quark correlations in hadron collisions at next-to-leading order,” *Nucl. Phys.* **B373** (1992) 295–345.
- [9] E. Norrbin and T. Sjostrand, “Production and hadronization of heavy quarks,” *Eur. Phys. J.* **C17** (2000) 137–161, arXiv:hep-ph/0005110 [hep-ph].
- [10] LHCb Collaboration, R. Aaij *et al.*, “Observation of double charm production involving open charm in pp collisions at $\sqrt{s} = 7$ TeV,” *JHEP* **06** (2012) 141, arXiv:1205.0975 [hep-ex]. [Addendum: *JHEP* **03** (2014) 108].
- [11] STAR Collaboration, M. M. Aggarwal *et al.*, “Measurement of the Bottom contribution to non-photonic electron production in $p + p$ collisions at $\sqrt{s}=200$ GeV,” *Phys. Rev. Lett.* **105** (2010) 202301, arXiv:1007.1200 [nucl-ex].
- [12] ALICE Collaboration, B. B. Abelev *et al.*, “Beauty production in pp collisions at $\sqrt{s} = 2.76$ TeV measured via semi-electronic decays,” *Phys. Lett.* **B738** (2014) 97–108, arXiv:1405.4144 [nucl-ex].
- [13] STAR Collaboration, J. Adams *et al.*, “Evidence from d + Au measurements for final state suppression of high p(T) hadrons in Au+Au collisions at RHIC,” *Phys. Rev. Lett.* **91** (2003) 072304, arXiv:nucl-ex/0306024 [nucl-ex].
- [14] PHENIX Collaboration, A. Adare *et al.*, “Trends in Yield and Azimuthal Shape Modification in Dihadron Correlations in Relativistic Heavy Ion Collisions,” *Phys. Rev. Lett.* **104** (2010) 252301, arXiv:1002.1077 [nucl-ex].
- [15] ALICE Collaboration, K. Aamodt *et al.*, “Particle-yield modification in jet-like azimuthal di-hadron correlations in Pb-Pb collisions at $\sqrt{s_{NN}} = 2.76$ TeV,” *Phys. Rev. Lett.* **108** (2012) 092301, arXiv:1110.0121 [nucl-ex].
- [16] ALICE Collaboration, K. Aamodt *et al.*, “Elliptic flow of charged particles in Pb-Pb collisions at $\sqrt{s_{NN}} = 2.76$ TeV,” *Phys. Rev. Lett.* **105** (2010) 252302, arXiv:1011.3914 [nucl-ex].
- [17] ALICE Collaboration, K. Aamodt *et al.*, “Higher harmonic anisotropic flow measurements of charged particles in Pb-Pb collisions at $\sqrt{s_{NN}}=2.76$ TeV,” *Phys. Rev. Lett.* **107** (2011) 032301, arXiv:1105.3865 [nucl-ex].
- [18] CMS Collaboration, V. Khachatryan *et al.*, “Observation of Long-Range Near-Side Angular Correlations in Proton-Proton Collisions at the LHC,” *JHEP* **09** (2010) 091, arXiv:1009.4122 [hep-ex].
- [19] ATLAS Collaboration, G. Aad *et al.*, “Observation of long-range elliptic anisotropies in $\sqrt{s} = 13$ and 2.76 TeV pp collisions with the ATLAS detector,” *Phys. Rev. Lett.* **116** (2016) 172301, arXiv:1509.04776 [hep-ex].
- [20] ALICE Collaboration, B. Abelev *et al.*, “Long-range angular correlations on the near and away

- side in p–Pb collisions at $\sqrt{s_{NN}} = 5.02$ TeV,” *Phys. Lett.* **B719** (2013) 29–41, arXiv:1212.2001 [nucl-ex].
- [21] ALICE Collaboration, J. Adam *et al.*, “Forward-central two-particle correlations in p–Pb collisions at $\sqrt{s_{NN}} = 5.02$ TeV,” *Phys. Lett.* **B753** (2016) 126–139, arXiv:1506.08032 [nucl-ex].
- [22] ATLAS Collaboration, G. Aad *et al.*, “Observation of Associated Near-Side and Away-Side Long-Range Correlations in $\sqrt{s_{NN}} = 5.02$ TeV Proton-Lead Collisions with the ATLAS Detector,” *Phys. Rev. Lett.* **110** (2013) 182302, arXiv:1212.5198 [hep-ex].
- [23] CMS Collaboration, V. Khachatryan *et al.*, “Evidence for Collective Multiparticle Correlations in p–Pb Collisions,” *Phys. Rev. Lett.* **115** no. 1, (2015) 012301, arXiv:1502.05382 [nucl-ex].
- [24] PHENIX Collaboration, A. Adare *et al.*, “Quadrupole Anisotropy in Dihadron Azimuthal Correlations in Central $d+Au$ Collisions at $\sqrt{s_{NN}}=200$ GeV,” *Phys. Rev. Lett.* **111** no. 21, (2013) 212301, arXiv:1303.1794 [nucl-ex].
- [25] STAR Collaboration, L. Adamczyk *et al.*, “Long-range pseudorapidity dihadron correlations in $d+Au$ collisions at $\sqrt{s_{NN}} = 200$ GeV,” *Phys. Lett.* **B747** (2015) 265–271, arXiv:1502.07652 [nucl-ex].
- [26] STAR Collaboration, L. Adamczyk *et al.*, “Effect of event selection on jetlike correlation measurement in $d+Au$ collisions at $\sqrt{s_{NN}} = 200$ GeV,” *Phys. Lett.* **B743** (2015) 333–339, arXiv:1412.8437 [nucl-ex].
- [27] K. Werner, I. Karpenko, and T. Pierog, “‘Ridge’ in Proton-Proton Scattering at 7 TeV,” *Phys. Rev. Lett.* **106** (2011) 122004, arXiv:1011.0375 [hep-ph].
- [28] S. Alderweireldt and P. Van Mechelen, “Obtaining the CMS Ridge effect with Multiparton Interactions,” in *Proceedings, 3rd International Workshop on Multiple Partonic Interactions at the LHC (MPI@LHC 2011)*, pp. 33–40. 2012. arXiv:1203.2048 [hep-ph]. <http://inspirehep.net/record/1093441/files/arXiv:1203.2048.pdf>.
- [29] P. Bozek and W. Broniowski, “Collective dynamics in high-energy proton-nucleus collisions,” *Phys. Rev.* **C88** (2013) 014903, arXiv:1304.3044 [nucl-th].
- [30] P. Bozek and W. Broniowski, “Correlations from hydrodynamic flow in p–Pb collisions,” *Phys. Lett.* **B718** (2013) 1557–1561, arXiv:1211.0845 [nucl-th].
- [31] L. He, T. Edmonds, Z.-W. Lin, F. Liu, D. Molnar, and F. Wang, “Anisotropic parton escape is the dominant source of azimuthal anisotropy in transport models,” *Phys. Lett.* **B753** (2016) 506–510, arXiv:1502.05572 [nucl-th].
- [32] K. Dusling and R. Venugopalan, “Comparison of the color glass condensate to dihadron correlations in proton-proton and proton-nucleus collisions,” *Phys. Rev.* **D87** (2013) 094034, arXiv:1302.7018 [hep-ph].
- [33] B. A. Arbuzov, E. E. Boos, and V. I. Savrin, “CMS ridge effect at LHC as a manifestation of bremsstrahlung of gluons due to the quark-antiquark string formation,” *Eur. Phys. J.* **C71** (2011) 1730, arXiv:1104.1283 [hep-ph].
- [34] ALICE Collaboration, B. B. Abelev *et al.*, “Measurement of prompt D -meson production in $p - Pb$ collisions at $\sqrt{s_{NN}} = 5.02$ TeV,” *Phys. Rev. Lett.* **113** no. 23, (2014) 232301, arXiv:1405.3452 [nucl-ex].
- [35] PHENIX Collaboration, A. Adare *et al.*, “Heavy-flavor electron-muon correlations in $p+p$ and $d+Au$ collisions at $\sqrt{s_{NN}} = 200$ GeV,” *Phys. Rev.* **C89** (2014) 034915, arXiv:1311.1427 [nucl-ex].
- [36] H. Fujii and K. Watanabe, “Heavy quark pair production in high energy pA collisions: Open heavy flavors,” *Nucl. Phys.* **A920** (2013) 78–93, arXiv:1308.1258 [hep-ph].
- [37] A. Beraudo, A. De Pace, M. Monteno, M. Nardi, and F. Prino, “Heavy-flavour production in

- high-energy d–Au and p–Pb collisions,” *JHEP* **1603** (2016) 123, arXiv:1512.05186 [hep-ph].
- [38] Y. Xu, S. Cao, G.-Y. Qin, W. Ke, M. Nahrgang, J. Auvinen, and S. A. Bass, “Heavy-flavor dynamics in relativistic p–Pb collisions at $\sqrt{s_{NN}} = 5.02$ TeV,” arXiv:1510.07520 [nucl-th].
- [39] PHENIX Collaboration, A. Adare *et al.*, “Cold-nuclear-matter effects on heavy-quark production in d+Au collisions at $\sqrt{s_{NN}} = 200$ GeV,” *Phys. Rev. Lett.* **109** (2012) 242301, arXiv:1208.1293 [nucl-ex].
- [40] P. Bozek, A. Bzdak, and G.-L. Ma, “Rapidity dependence of elliptic and triangular flow in protonnucleus collisions from collective dynamics,” *Phys. Lett.* **B748** (2015) 301–305, arXiv:1503.03655 [hep-ph].
- [41] ALICE Collaboration, K. Aamodt *et al.*, “The ALICE experiment at the CERN LHC,” *JINST* **3** (2008) S08002.
- [42] ALICE Collaboration, B. B. Abelev *et al.*, “Performance of the ALICE Experiment at the CERN LHC,” *Int. J. Mod. Phys.* **A29** (2014) 1430044, arXiv:1402.4476 [nucl-ex].
- [43] P. Z. Skands, “Tuning Monte Carlo Generators: The Perugia Tunes,” *Phys. Rev.* **D82** (2010) 074018, arXiv:1005.3457 [hep-ph].
- [44] X.-N. Wang and M. Gyulassy, “HIJING: A Monte Carlo model for multiple jet production in p p, p A and A A collisions,” *Phys. Rev.* **D44** (1991) 3501–3516.
- [45] R. Brun, F. Carminati, and S. Giani, “GEANT Detector Description and Simulation Tool,” *CERN Program Library Long Write-up W5013* (1994).
- [46] T. Sjostrand, S. Mrenna, and P. Z. Skands, “A Brief Introduction to PYTHIA 8.1,” *Comput. Phys. Commun.* **178** (2008) 852–867, arXiv:0710.3820 [hep-ph].
- [47] P. Nason, “A New method for combining NLO QCD with shower Monte Carlo algorithms,” *JHEP* **11** (2004) 040, arXiv:hep-ph/0409146 [hep-ph].
- [48] S. Frixione, P. Nason, and C. Oleari, “Matching NLO QCD computations with Parton Shower simulations: the POWHEG method,” *JHEP* **11** (2007) 070, arXiv:0709.2092 [hep-ph].
- [49] M. Cacciari, S. Frixione, N. Houdeau, M. L. Mangano, P. Nason, and G. Ridolfi, “Theoretical predictions for charm and bottom production at the LHC,” *JHEP* **10** (2012) 137, arXiv:1205.6344 [hep-ph].
- [50] M. Klasen, C. Klein-Bösing, K. Kovaric, G. Kramer, M. Topp, and J. P. Wessels, “NLO Monte Carlo predictions for heavy-quark production at the LHC: pp collisions in ALICE,” *JHEP* **08** (2014) 109, arXiv:1405.3083 [hep-ph].
- [51] S. Alioli, P. Nason, C. Oleari, and E. Re, “A general framework for implementing NLO calculations in shower Monte Carlo programs: the POWHEG BOX,” *JHEP* **06** (2010) 043, arXiv:1002.2581 [hep-ph].
- [52] S. Frixione, P. Nason, and G. Ridolfi, “A Positive-weight next-to-leading-order Monte Carlo for heavy flavour hadroproduction,” *JHEP* **09** (2007) 126, arXiv:0707.3088 [hep-ph].
- [53] H.-L. Lai, M. Guzzi, J. Huston, Z. Li, P. M. Nadolsky, J. Pumplin, and C. P. Yuan, “New parton distributions for collider physics,” *Phys. Rev.* **D82** (2010) 074024, arXiv:1007.2241 [hep-ph].
- [54] K. J. Eskola, H. Paukkunen, and C. A. Salgado, “EPS09: A New Generation of NLO and LO Nuclear Parton Distribution Functions,” *JHEP* **04** (2009) 065, arXiv:0902.4154 [hep-ph].
- [55] Particle Data Group Collaboration, K. A. Olive *et al.*, “Review of Particle Physics (RPP),” *Chin. Phys.* **C38** (2014) 090001.

A The ALICE Collaboration

J. Adam³⁹, D. Adamová⁸⁵, M.M. Aggarwal⁸⁹, G. Aglieri Rinella³⁵, M. Agnello¹¹¹, N. Agrawal⁴⁸, Z. Ahammed¹³⁴, S. Ahmad¹⁹, S.U. Ahn⁶⁹, S. Aiola¹³⁸, A. Akindinov⁵⁹, S.N. Alam¹³⁴, D.S.D. Albuquerque¹²², D. Aleksandrov⁸¹, B. Alessandro¹¹¹, D. Alexandre¹⁰², R. Alfaro Molina⁶⁵, A. Alici^{105,12}, A. Alkin³, J.R.M. Almaraz¹²⁰, J. Alme^{37,18}, T. Alt⁴², S. Altinpinar¹⁸, I. Altsybeev¹³³, C. Alves Garcia Prado¹²¹, C. Andrei⁷⁹, A. Andronic⁹⁸, V. Anguelov⁹⁵, T. Antičić⁹⁹, F. Antinori¹⁰⁸, P. Antonioli¹⁰⁵, L. Aphecetche¹¹⁴, H. Appelshäuser⁵⁴, S. Arcelli²⁷, R. Arnaldi¹¹¹, O.W. Arnold^{94,36}, I.C. Arsene²², M. Arslanok⁵⁴, B. Audurier¹¹⁴, A. Augustinus³⁵, R. Averbeck⁹⁸, M.D. Azmi¹⁹, A. Badalà¹⁰⁷, Y.W. Baek⁶⁸, S. Bagnasco¹¹¹, R. Bailhache⁵⁴, R. Bala⁹², S. Balasubramanian¹³⁸, A. Baldissieri¹⁵, R.C. Baral⁶², A.M. Barbano²⁶, R. Barbera²⁸, F. Barile³², G.G. Barnaföldi¹³⁷, L.S. Barnby^{102,35}, V. Barret⁷¹, P. Bartalini⁷, K. Barth³⁵, J. Bartke^{118,i}, E. Bartsch⁵⁴, M. Basile²⁷, N. Bastid⁷¹, S. Basu¹³⁴, B. Bathen⁵⁵, G. Batigne¹¹⁴, A. Batista Camejo⁷¹, B. Batyunya⁶⁷, P.C. Batzing²², I.G. Bearden⁸², H. Beck^{54,95}, C. Bedda¹¹¹, N.K. Behera⁵¹, I. Belikov⁵⁶, F. Bellini²⁷, H. Bello Martinez², R. Bellwied¹²³, R. Belmont¹³⁶, E. Belmont-Moreno⁶⁵, L.G.E. Beltran¹²⁰, V. Belyaev⁷⁶, G. Bencedi¹³⁷, S. Beole²⁶, I. Berceanu⁷⁹, A. Bercuci⁷⁹, Y. Berdnikov⁸⁷, D. Berenyi¹³⁷, R.A. Bertens⁵⁸, D. Berzano³⁵, L. Betev³⁵, A. Bhasin⁹², I.R. Bhat⁹², A.K. Bhati⁸⁹, B. Bhattacharjee⁴⁴, J. Bhom¹¹⁸, L. Bianchi¹²³, N. Bianchi⁷³, C. Bianchin¹³⁶, J. Bielčik³⁹, J. Bielčiková⁸⁵, A. Bilandzic^{82,36,94}, G. Biro¹³⁷, R. Biswas⁴, S. Biswas^{4,80}, S. Bjelogrić⁵⁸, J.T. Blair¹¹⁹, D. Blau⁸¹, C. Blume⁵⁴, F. Bock^{75,95}, A. Bogdanov⁷⁶, H. Bøggild⁸², L. Boldizsár¹³⁷, M. Bombara⁴⁰, M. Bonora³⁵, J. Book⁵⁴, H. Borel¹⁵, A. Borissov⁹⁷, M. Borri^{125,84}, F. Bossú⁶⁶, E. Botta²⁶, C. Bourjau⁸², P. Braun-Munzinger⁹⁸, M. Bregant¹²¹, T. Breitner⁵³, T.A. Broker⁵⁴, T.A. Browning⁹⁶, M. Broz³⁹, E.J. Brucken⁴⁶, E. Bruna¹¹¹, G.E. Bruno³², D. Budnikov¹⁰⁰, H. Buesching⁵⁴, S. Bufalino^{35,26}, P. Buncic³⁵, O. Busch¹²⁹, Z. Buthelezi⁶⁶, J.B. Butt¹⁶, J.T. Buxton²⁰, J. Cabala¹¹⁶, D. Caffarri³⁵, X. Cai⁷, H. Caines¹³⁸, L. Calero Diaz⁷³, A. Caliva⁵⁸, E. Calvo Villar¹⁰³, P. Camerini²⁵, F. Carena³⁵, W. Carena³⁵, F. Carnesecchi²⁷, J. Castillo Castellanos¹⁵, A.J. Castro¹²⁶, E.A.R. Casula²⁴, C. Ceballos Sanchez⁹, J. Cepila³⁹, P. Cerello¹¹¹, J. Cerkala¹¹⁶, B. Chang¹²⁴, S. Chapeland³⁵, M. Chartier¹²⁵, J.L. Charvet¹⁵, S. Chattopadhyay¹³⁴, S. Chattopadhyay¹⁰¹, A. Chauvin^{94,36}, V. Chelnokov³, M. Cherney⁸⁸, C. Cheshkov¹³¹, B. Cheynis¹³¹, V. Chibante Barroso³⁵, D.D. Chinellato¹²², S. Cho⁵¹, P. Chochula³⁵, K. Choi⁹⁷, M. Chojnacki⁸², S. Choudhury¹³⁴, P. Christakoglou⁸³, C.H. Christensen⁸², P. Christiansen³³, T. Chujo¹²⁹, S.U. Chung⁹⁷, C. Cicalo¹⁰⁶, L. Cifarelli^{12,27}, F. Cindolo¹⁰⁵, J. Cleymans⁹¹, F. Colamaria³², D. Colella^{60,35}, A. Collu⁷⁵, M. Colocci²⁷, G. Conesa Balbastre⁷², Z. Conesa del Valle⁵², M.E. Connors^{ii,138}, J.G. Contreras³⁹, T.M. Cormier⁸⁶, Y. Corrales Morales^{26,111}, I. Cortés Maldonado², P. Cortese³¹, M.R. Cosentino¹²¹, F. Costa³⁵, J. Crkovska⁵², P. Crochet⁷¹, R. Cruz Albino¹¹, E. Cuautle⁶⁴, L. Cunqueiro^{55,35}, T. Dahms^{94,36}, A. Dainese¹⁰⁸, M.C. Danisch⁹⁵, A. Danu⁶³, D. Das¹⁰¹, I. Das¹⁰¹, S. Das⁴, A. Dash⁸⁰, S. Dash⁴⁸, S. De¹²¹, A. De Caro^{12,30}, G. de Cataldo¹⁰⁴, C. de Conti¹²¹, J. de Cuveland⁴², A. De Falco²⁴, D. De Gruttola^{12,30}, N. De Marco¹¹¹, S. De Pasquale³⁰, R.D. De Souza¹²², A. Deisting^{95,98}, A. Deloff⁷⁸, E. Dénes^{137,i}, C. Deplano⁸³, P. Dhankher⁴⁸, D. Di Bari³², A. Di Mauro³⁵, P. Di Nezza⁷³, B. Di Ruzza¹⁰⁸, M.A. Diaz Corchero¹⁰, T. Dietel⁹¹, P. Dillenseger⁵⁴, R. Diviá³⁵, Ø. Djuvsland¹⁸, A. Dobrin^{83,63}, D. Domenicis Gimenez¹²¹, B. Dönigus⁵⁴, O. Dordic²², T. Drozhzhova⁵⁴, A.K. Dubey¹³⁴, A. Dubla⁵⁸, L. Ducroux¹³¹, P. Dupieux⁷¹, R.J. Ehlers¹³⁸, D. Elia¹⁰⁴, E. Endress¹⁰³, H. Engel⁵³, E. Epple¹³⁸, B. Erasmus¹¹⁴, I. Erdemir⁵⁴, F. Erhardt¹³⁰, B. Espagnon⁵², M. Estienne¹¹⁴, S. Esumi¹²⁹, J. Eum⁹⁷, D. Evans¹⁰², S. Evdokimov¹¹², G. Eyyubova³⁹, L. Fabbietti^{94,36}, D. Fabris¹⁰⁸, J. Faivre⁷², A. Fantoni⁷³, M. Fasel⁷⁵, L. Feldkamp⁵⁵, A. Feliciello¹¹¹, G. Feofilov¹³³, J. Ferencei⁸⁵, A. Fernández Téllez², E.G. Ferreira¹⁷, A. Ferretti²⁶, A. Festanti²⁹, V.J.G. Feuillard^{15,71}, J. Figiel¹¹⁸, M.A.S. Figueredo^{125,121}, S. Filchagin¹⁰⁰, D. Finogeev⁵⁷, F.M. Fionda²⁴, E.M. Fiore³², M.G. Fleck⁹⁵, M. Floris³⁵, S. Foertsch⁶⁶, P. Foka⁹⁸, S. Fokin⁸¹, E. Fragiaco¹¹⁰, A. Francescon³⁵, A. Francisco¹¹⁴, U. Frankenfeld⁹⁸, G.G. Fronze²⁶, U. Fuchs³⁵, C. Furget⁷², A. Furs⁵⁷, M. Fusco Girard³⁰, J.J. Gaardhøje⁸², M. Gagliardi²⁶, A.M. Gago¹⁰³, K. Gajdosova⁸², M. Gallio²⁶, C.D. Galvan¹²⁰, D.R. Gangadharan⁷⁵, P. Ganoti⁹⁰, C. Gao⁷, C. Garabatos⁹⁸, E. Garcia-Solis¹³, C. Gargiulo³⁵, P. Gasik^{94,36}, E.F. Gauger¹¹⁹, M. Germain¹¹⁴, M. Gheata^{35,63}, P. Ghosh¹³⁴, S.K. Ghosh⁴, P. Gianotti⁷³, P. Giubellino^{111,35}, P. Giubilato²⁹, E. Gladysz-Dziadus¹¹⁸, P. Glässel⁹⁵, D.M. Gómez Coral⁶⁵, A. Gomez Ramirez⁵³, A.S. Gonzalez³⁵, V. Gonzalez¹⁰, P. González-Zamora¹⁰, S. Gorbunov⁴², L. Görlich¹¹⁸, S. Gotovac¹¹⁷, V. Grabski⁶⁵, O.A. Grachov¹³⁸, L.K. Graczykowski¹³⁵, K.L. Graham¹⁰², A. Grelli⁵⁸, A. Grigoras³⁵, C. Grigoras³⁵, V. Grigoriev⁷⁶, A. Grigoryan¹, S. Grigoryan⁶⁷, B. Grinyov³, N. Grion¹¹⁰, J.M. Gronefeld⁹⁸, J.F. Grosse-Oetringhaus³⁵, R. Grosso⁹⁸, L. Gruber¹¹³, F. Guber⁵⁷, R. Guernane⁷², B. Guerzoni²⁷, K. Gulbrandsen⁸², T. Gunji¹²⁸, A. Gupta⁹², R. Gupta⁹², R. Haake³⁵, C. Hadjidakis⁵², M. Haiduc⁶³, H. Hamagaki¹²⁸, G. Hamar¹³⁷, J.C. Hamon⁵⁶, J.W. Harris¹³⁸, A. Harton¹³, D. Hatzifotiadou¹⁰⁵, S. Hayashi¹²⁸, S.T. Heckel⁵⁴, E. Hellbär⁵⁴, H. Helstrup³⁷, A. Herghelegiu⁷⁹, G. Herrera Corral¹¹, B.A. Hess³⁴,

K.F. Hetland³⁷, H. Hillemanns³⁵, B. Hippolyte⁵⁶, D. Horak³⁹, R. Hosokawa¹²⁹, P. Hristov³⁵, C. Hughes¹²⁶, T.J. Humanic²⁰, N. Hussain⁴⁴, T. Hussain¹⁹, D. Hutter⁴², D.S. Hwang²¹, R. Ilkaev¹⁰⁰, M. Inaba¹²⁹, E. Incani²⁴, M. Ippolitov^{76,81}, M. Irfan¹⁹, V. Isakov⁵⁷, M. Ivanov⁹⁸, V. Ivanov⁸⁷, V. Izucheev¹¹², B. Jacak⁷⁵, N. Jacazio²⁷, P.M. Jacobs⁷⁵, M.B. Jadhav⁴⁸, S. Jadlovská¹¹⁶, J. Jadlovsky^{116,60}, C. Jahnke¹²¹, M.J. Jakubowska¹³⁵, M.A. Janik¹³⁵, P.H.S.Y. Jayarathna¹²³, C. Jena²⁹, S. Jena¹²³, R.T. Jimenez Bustamante⁹⁸, P.G. Jones¹⁰², A. Jusko¹⁰², P. Kalinak⁶⁰, A. Kalweit³⁵, J.H. Kang¹³⁹, V. Kaplin⁷⁶, S. Kar¹³⁴, A. Karasu Uysal⁷⁰, O. Karavichev⁵⁷, T. Karavicheva⁵⁷, L. Karayan^{98,95}, E. Karpechev⁵⁷, U. Kebschull⁵³, R. Keidel¹⁴⁰, D.L.D. Keijdener⁵⁸, M. Keil³⁵, M. Mohisin Khan^{iii,19}, P. Khan¹⁰¹, S.A. Khan¹³⁴, A. Khanzadeev⁸⁷, Y. Kharlov¹¹², B. Kileng³⁷, D.W. Kim⁴³, D.J. Kim¹²⁴, D. Kim¹³⁹, H. Kim¹³⁹, J.S. Kim⁴³, J. Kim⁹⁵, M. Kim¹³⁹, S. Kim²¹, T. Kim¹³⁹, S. Kirsch⁴², I. Kisel⁴², S. Kiselev⁵⁹, A. Kisiel¹³⁵, G. Kiss¹³⁷, J.L. Klay⁶, C. Klein⁵⁴, J. Klein³⁵, C. Klein-Bösing⁵⁵, S. Klewin⁹⁵, A. Kluge³⁵, M.L. Knichel⁹⁵, A.G. Knospe^{119,123}, C. Kobdaj¹¹⁵, M. Kofarago³⁵, T. Kollegger⁹⁸, A. Kolojvari¹³³, V. Kondratiev¹³³, N. Kondratyeva⁷⁶, E. Kondratyuk¹¹², A. Konevskikh⁵⁷, M. Kopicik¹¹⁶, M. Kour⁹², C. Kouzinopoulos³⁵, O. Kovalenko⁷⁸, V. Kovalenko¹³³, M. Kowalski¹¹⁸, G. Koyithatta Meethalevedu⁴⁸, I. Králik⁶⁰, A. Kravčáková⁴⁰, M. Krivda^{60,102}, F. Krizek⁸⁵, E. Kryshen^{87,35}, M. Krzewicki⁴², A.M. Kubera²⁰, V. Kučera⁸⁵, C. Kuhn⁵⁶, P.G. Kuijer⁸³, A. Kumar⁹², J. Kumar⁴⁸, L. Kumar⁸⁹, S. Kumar⁴⁸, P. Kurashvili⁷⁸, A. Kurepin⁵⁷, A.B. Kurepin⁵⁷, A. Kuryakin¹⁰⁰, M.J. Kweon⁵¹, Y. Kwon¹³⁹, S.L. La Pointe¹¹¹, P. La Rocca²⁸, P. Ladron de Guevara¹¹, C. Lagana Fernandes¹²¹, I. Lakomov³⁵, R. Langoy⁴¹, K. Lapidus^{138,36}, C. Lara⁵³, A. Lardeux¹⁵, A. Lattuca²⁶, E. Laudi³⁵, R. Lea²⁵, L. Leardini⁹⁵, S. Lee¹³⁹, F. Lehas⁸³, S. Lehner¹¹³, R.C. Lemmon⁸⁴, V. Lenti¹⁰⁴, E. Leogrande⁵⁸, I. León Monzón¹²⁰, H. León Vargas⁶⁵, M. Leoncino²⁶, P. Lévai¹³⁷, S. Li^{71,7}, X. Li¹⁴, J. Lien⁴¹, R. Lietava¹⁰², S. Lindal²², V. Lindenstruth⁴², C. Lippmann⁹⁸, M.A. Lisa²⁰, H.M. Ljunggren³³, D.F. Lodato⁵⁸, P.I. Loenne¹⁸, V. Loginov⁷⁶, C. Loizides⁷⁵, X. Lopez⁷¹, E. López Torres⁹, A. Lowe¹³⁷, P. Luettig⁵⁴, M. Lunardon²⁹, G. Luparello²⁵, M. Lupi³⁵, T.H. Lutz¹³⁸, A. Maevskaya⁵⁷, M. Mager³⁵, S. Mahajan⁹², S.M. Mahmood²², A. Maire⁵⁶, R.D. Majka¹³⁸, M. Malaev⁸⁷, I. Maldonado Cervantes⁶⁴, L. Malinina^{iv,67}, D. Mal'Kevich⁵⁹, P. Malzacher⁹⁸, A. Mamonov¹⁰⁰, V. Manko⁸¹, F. Manso⁷¹, V. Manzari^{104,35}, Y. Mao⁷, M. Marchisone^{26,127,66}, J. Mareš⁶¹, G.V. Margagliotti²⁵, A. Margotti¹⁰⁵, J. Margutti⁵⁸, A. Marín⁹⁸, C. Markert¹¹⁹, M. Marquard⁵⁴, N.A. Martin⁹⁸, P. Martinengo³⁵, M.I. Martínez², G. Martínez García¹¹⁴, M. Martinez Pedreira³⁵, A. Mas¹²¹, S. Masciocchi⁹⁸, M. Maserà²⁶, A. Masoni¹⁰⁶, A. Mastroserio³², A. Matyja¹¹⁸, C. Mayer¹¹⁸, J. Mazer¹²⁶, M.A. Mazzoni¹⁰⁹, D. McDonald¹²³, F. Meddi²³, Y. Melikyan⁷⁶, A. Menchaca-Rocha⁶⁵, E. Meninno³⁰, J. Mercado Pérez⁹⁵, M. Meres³⁸, S. Mhlanga⁹¹, Y. Miake¹²⁹, M.M. Mieskolainen⁴⁶, K. Mikhaylov^{59,67}, L. Milano^{35,75}, J. Milosevic²², A. Mischke⁵⁸, A.N. Mishra⁴⁹, D. Miśkowiec⁹⁸, J. Mitra¹³⁴, C.M. Mitu⁶³, N. Mohammadi⁵⁸, B. Mohanty⁸⁰, L. Molnar⁵⁶, L. Montaño Zetina¹¹, E. Montes¹⁰, D.A. Moreira De Godoy⁵⁵, L.A.P. Moreno², S. Moretto²⁹, A. Morreale¹¹⁴, A. Morsch³⁵, V. Muccifora⁷³, E. Mudnic¹¹⁷, D. Mühlheim⁵⁵, S. Muhuri¹³⁴, M. Mukherjee¹³⁴, J.D. Mulligan¹³⁸, M.G. Munhoz¹²¹, K. Münnig⁴⁵, R.H. Munzer^{94,36,54}, H. Murakami¹²⁸, S. Murray⁶⁶, L. Musa³⁵, J. Musinsky⁶⁰, B. Naik⁴⁸, R. Nair⁷⁸, B.K. Nandi⁴⁸, R. Nania¹⁰⁵, E. Nappi¹⁰⁴, M.U. Naru¹⁶, H. Natal da Luz¹²¹, C. Natrass¹²⁶, S.R. Navarro², K. Nayak⁸⁰, R. Nayak⁴⁸, T.K. Nayak¹³⁴, S. Nazarenko¹⁰⁰, A. Nedosekin⁵⁹, R.A. Negrao De Oliveira³⁵, L. Nellen⁶⁴, F. Ng¹²³, M. Nicassio⁹⁸, M. Niculescu⁶³, J. Niedziela³⁵, B.S. Nielsen⁸², S. Nikolaev⁸¹, S. Nikulin⁸¹, V. Nikulin⁸⁷, F. Noferini^{105,12}, P. Nomokonov⁶⁷, G. Nooren⁵⁸, J.C.C. Noris², J. Norman¹²⁵, A. Nyanin⁸¹, J. Nystrand¹⁸, H. Oeschler⁹⁵, S. Oh¹³⁸, S.K. Oh⁶⁸, A. Ohlson³⁵, A. Okatan⁷⁰, T. Okubo⁴⁷, J. Oleniacz¹³⁵, A.C. Oliveira Da Silva¹²¹, M.H. Oliver¹³⁸, J. Onderwaater⁹⁸, C. Oppedisano¹¹¹, R. Orava⁴⁶, M. Oravec¹¹⁶, A. Ortiz Velasquez⁶⁴, A. Oskarsson³³, J. Otwinowski¹¹⁸, K. Oyama^{95,77}, M. Ozdemir⁵⁴, Y. Pachmayer⁹⁵, D. Pagano¹³², P. Pagano³⁰, G. Paic⁶⁴, S.K. Pal¹³⁴, P. Paini⁷, J. Pan¹³⁶, A.K. Pandey⁴⁸, V. Papikyan¹, G.S. Pappalardo¹⁰⁷, P. Pareek⁴⁹, W.J. Park⁹⁸, S. Parmar⁸⁹, A. Passfeld⁵⁵, V. Paticchio¹⁰⁴, R.N. Patra¹³⁴, B. Paul^{111,101}, H. Pei⁷, T. Peitzmann⁵⁸, X. Peng⁷, H. Pereira Da Costa¹⁵, D. Peresunko^{81,76}, E. Perez Lezama⁵⁴, V. Peskov⁵⁴, Y. Pestov⁵, V. Petráček³⁹, V. Petrov¹¹², M. Petrovici⁷⁹, C. Petta²⁸, S. Piano¹¹⁰, M. Pikna³⁸, P. Pillot¹¹⁴, L.O.D.L. Pimentel⁸², O. Pinazza^{105,35}, L. Pinsky¹²³, D.B. Piyarathna¹²³, M. Płoskoń⁷⁵, M. Planinic¹³⁰, J. Pluta¹³⁵, S. Pochybova¹³⁷, P.L.M. Podesta-Lerma¹²⁰, M.G. Poghosyan^{86,88}, B. Polichtchouk¹¹², N. Poljak¹³⁰, W. Poonsawat¹¹⁵, A. Pop⁷⁹, H. Poppenborg⁵⁵, S. Porteboeuf-Houssais⁷¹, J. Porter⁷⁵, J. Pospisil⁸⁵, S.K. Prasad⁴, R. Preghenella^{105,35}, F. Prino¹¹¹, C.A. Pruneau¹³⁶, I. Pshenichnov⁵⁷, M. Puccio²⁶, G. Puddu²⁴, P. Pujahari¹³⁶, V. Punin¹⁰⁰, J. Putschke¹³⁶, H. Qvigstad²², A. Rachevski¹¹⁰, S. Raha⁴, S. Rajput⁹², J. Rak¹²⁴, A. Rakotozafindrabe¹⁵, L. Ramello³¹, F. Rami⁵⁶, R. Raniwala⁹³, S. Raniwala⁹³, S.S. Räsänen⁴⁶, B.T. Rascanu⁵⁴, D. Rathee⁸⁹, K.F. Read^{126,86}, K. Redlich⁷⁸, R.J. Reed¹³⁶, A. Rehman¹⁸, P. Reichelt⁵⁴, F. Reidt^{35,95}, X. Ren⁷, R. Renfordt⁵⁴, A.R. Reolon⁷³, A. Reshetin⁵⁷, K. Reygers⁹⁵, V. Riabov⁸⁷, R.A. Ricci⁷⁴, T. Richert³³, M. Richter²², P. Riedler³⁵, W. Riegler³⁵, F. Riggi²⁸, C. Ristea⁶³, E. Rocco⁵⁸, M. Rodríguez

Cahuantzi², A. Rodriguez Manso⁸³, K. Røed²², E. Rogochaya⁶⁷, D. Rohr⁴², D. Röhrich¹⁸, F. Ronchetti^{35,73}, L. Ronflette¹¹⁴, P. Rosnet⁷¹, A. Rossi²⁹, F. Roukoutakis⁹⁰, A. Roy⁴⁹, C. Roy⁵⁶, P. Roy¹⁰¹, A.J. Rubio Montero¹⁰, R. Rui²⁵, R. Russo²⁶, E. Ryabinkin⁸¹, Y. Ryabov⁸⁷, A. Rybicki¹¹⁸, S. Saarinen⁴⁶, S. Sadhu¹³⁴, S. Sadovsky¹¹², K. Šafařík³⁵, B. Sahlmuller⁵⁴, P. Sahoo⁴⁹, R. Sahoo⁴⁹, S. Sahoo⁶², P.K. Sahu⁶², J. Saini¹³⁴, S. Sakai⁷³, M.A. Saleh¹³⁶, J. Salzwedel²⁰, S. Sambyal⁹², V. Samsonov^{76,87}, L. Šándor⁶⁰, A. Sandoval⁶⁵, M. Sano¹²⁹, D. Sarkar¹³⁴, N. Sarkar¹³⁴, P. Sarma⁴⁴, E. Scapparone¹⁰⁵, F. Scarlassara²⁹, C. Schiaua⁷⁹, R. Schicker⁹⁵, C. Schmidt⁹⁸, H.R. Schmidt³⁴, M. Schmidt³⁴, S. Schuchmann^{54,95}, J. Schukraft³⁵, Y. Schutz^{35,114}, K. Schwarz⁹⁸, K. Schweda⁹⁸, G. Scioli²⁷, E. Scomparin¹¹¹, R. Scott¹²⁶, M. Šefčík⁴⁰, J.E. Seger⁸⁸, Y. Sekiguchi¹²⁸, D. Sekihata⁴⁷, I. Selyuzhenkov⁹⁸, K. Senosi⁶⁶, S. Senyukov^{3,35}, E. Serradilla^{10,65}, A. Sevcenco⁶³, A. Shabanov⁵⁷, A. Shabetai¹¹⁴, O. Shadura³, R. Shahoyan³⁵, A. Shangaraev¹¹², A. Sharma⁹², M. Sharma⁹², M. Sharma⁹², N. Sharma¹²⁶, A.I. Sheikh¹³⁴, K. Shigaki⁴⁷, Q. Shou⁷, K. Shtejer^{9,26}, Y. Sibiriak⁸¹, S. Siddhanta¹⁰⁶, K.M. Sielewicz³⁵, T. Siemiarczuk⁷⁸, D. Silvermyr³³, C. Silvestre⁷², G. Simatovic¹³⁰, G. Simonetti³⁵, R. Singaraju¹³⁴, R. Singh⁸⁰, V. Singhal¹³⁴, T. Sinha¹⁰¹, B. Sitar³⁸, M. Sitta³¹, T.B. Skaali²², M. Slupecki¹²⁴, N. Smirnov¹³⁸, R.J.M. Snellings⁵⁸, T.W. Snellman¹²⁴, J. Song⁹⁷, M. Song¹³⁹, Z. Song⁷, F. Soramel²⁹, S. Sorensen¹²⁶, F. Sozzi⁹⁸, E. Spiriti⁷³, I. Sputowska¹¹⁸, M. Spyropoulou-Stassinaki⁹⁰, J. Stachel⁹⁵, I. Stan⁶³, P. Stankus⁸⁶, E. Stenlund³³, G. Steyn⁶⁶, J.H. Stiller⁹⁵, D. Stocco¹¹⁴, P. Strmen³⁸, A.A.P. Suaide¹²¹, T. Sugitate⁴⁷, C. Suire⁵², M. Suleymanov¹⁶, M. Suljic^{25,i}, R. Sultanov⁵⁹, M. Šumbera⁸⁵, S. Sumowidagdo⁵⁰, A. Szabo³⁸, I. Szarka³⁸, A. Szczepankiewicz¹³⁵, M. Szymanski¹³⁵, U. Tabassam¹⁶, J. Takahashi¹²², G.J. Tambave¹⁸, N. Tanaka¹²⁹, M. Tarhini⁵², M. Tariq¹⁹, M.G. Tarzila⁷⁹, A. Tauro³⁵, G. Tejada Muñoz², A. Telesca³⁵, K. Terasaki¹²⁸, C. Terrevoli²⁹, B. Teyssier¹³¹, J. Thäder⁷⁵, D. Thakur⁴⁹, D. Thomas¹¹⁹, R. Tieulent¹³¹, A. Tikhonov⁵⁷, A.R. Timmins¹²³, A. Toia⁵⁴, S. Trogolo²⁶, G. Trombetta³², V. Trubnikov³, W.H. Trzaska¹²⁴, T. Tsuji¹²⁸, A. Tumkin¹⁰⁰, R. Turrisi¹⁰⁸, T.S. Tveter²², K. Ullaland¹⁸, A. Uras¹³¹, G.L. Usai²⁴, A. Utrobicic¹³⁰, M. Vala⁶⁰, L. Valencia Palomo⁷¹, S. Vallero²⁶, J. Van Der Maarel⁵⁸, J.W. Van Hoorne^{35,113}, M. van Leeuwen⁵⁸, T. Vanat⁸⁵, P. Vande Vyvre³⁵, D. Varga¹³⁷, A. Vargas², M. Vargyas¹²⁴, R. Varma⁴⁸, M. Vasileiou⁹⁰, A. Vasiliev⁸¹, A. Vauthier⁷², O. Vázquez Doce^{94,36}, V. Vechernin¹³³, A.M. Veen⁵⁸, M. Veldhoen⁵⁸, A. Velure¹⁸, E. Vercellin²⁶, S. Vergara Limón², R. Vernet⁸, M. Verweij¹³⁶, L. Vickovic¹¹⁷, J. Viinikainen¹²⁴, Z. Vilakazi¹²⁷, O. Villalobos Baillie¹⁰², A. Villatoro Tello², A. Vinogradov⁸¹, L. Vinogradov¹³³, T. Virgili³⁰, V. Vislavicius³³, Y.P. Viyogi¹³⁴, A. Vodopyanov⁶⁷, M.A. Völkl⁹⁵, K. Voloshin⁵⁹, S.A. Voloshin¹³⁶, G. Volpe^{32,137}, B. von Haller³⁵, I. Vorobyev^{94,36}, D. Vranic^{98,35}, J. Vrláková⁴⁰, B. Vulpescu⁷¹, B. Wagner¹⁸, J. Wagner⁹⁸, H. Wang⁵⁸, M. Wang⁷, D. Watanabe¹²⁹, Y. Watanabe¹²⁸, M. Weber^{35,113}, S.G. Weber⁹⁸, D.F. Weiser⁹⁵, J.P. Wessels⁵⁵, U. Westerhoff⁵⁵, A.M. Whitehead⁹¹, J. Wiechula³⁴, J. Wikne²², G. Wilk⁷⁸, J. Wilkinson⁹⁵, G.A. Willems⁵⁵, M.C.S. Williams¹⁰⁵, B. Windelband⁹⁵, M. Winn⁹⁵, S. Yalcin⁷⁰, P. Yang⁷, S. Yano⁴⁷, Z. Yin⁷, H. Yokoyama¹²⁹, I.-K. Yoo⁹⁷, J.H. Yoon⁵¹, V. Yurchenko³, A. Zaborowska¹³⁵, V. Zaccaro⁸², A. Zaman¹⁶, C. Zampolli^{105,35}, H.J.C. Zanoli¹²¹, S. Zaporozhets⁶⁷, N. Zardoshti¹⁰², A. Zarochentsev¹³³, P. Závada⁶¹, N. Zaviyalov¹⁰⁰, H. Zbroszczyk¹³⁵, I.S. Zgura⁶³, M. Zhalov⁸⁷, H. Zhang^{18,7}, X. Zhang^{75,7}, Y. Zhang⁷, C. Zhang⁵⁸, Z. Zhang⁷, C. Zhao²², N. Zhigareva⁵⁹, D. Zhou⁷, Y. Zhou⁸², Z. Zhou¹⁸, H. Zhu^{18,7}, J. Zhu^{7,114}, A. Zichichi^{27,12}, A. Zimmermann⁹⁵, M.B. Zimmermann^{55,35}, G. Zinovjev³, M. Zyzak⁴²

Affiliation notes

- ⁱ Deceased
- ⁱⁱ Also at: Georgia State University, Atlanta, Georgia, United States
- ⁱⁱⁱ Also at: Also at Department of Applied Physics, Aligarh Muslim University, Aligarh, India
- ^{iv} Also at: M.V. Lomonosov Moscow State University, D.V. Skobeltsyn Institute of Nuclear, Physics, Moscow, Russia

Collaboration Institutes

- ¹ A.I. Alikhanyan National Science Laboratory (Yerevan Physics Institute) Foundation, Yerevan, Armenia
- ² Benemérita Universidad Autónoma de Puebla, Puebla, Mexico
- ³ Bogolyubov Institute for Theoretical Physics, Kiev, Ukraine
- ⁴ Bose Institute, Department of Physics and Centre for Astroparticle Physics and Space Science (CAPSS), Kolkata, India
- ⁵ Budker Institute for Nuclear Physics, Novosibirsk, Russia
- ⁶ California Polytechnic State University, San Luis Obispo, California, United States
- ⁷ Central China Normal University, Wuhan, China

- ⁸ Centre de Calcul de l'IN2P3, Villeurbanne, France
- ⁹ Centro de Aplicaciones Tecnológicas y Desarrollo Nuclear (CEADEN), Havana, Cuba
- ¹⁰ Centro de Investigaciones Energéticas Medioambientales y Tecnológicas (CIEMAT), Madrid, Spain
- ¹¹ Centro de Investigación y de Estudios Avanzados (CINVESTAV), Mexico City and Mérida, Mexico
- ¹² Centro Fermi - Museo Storico della Fisica e Centro Studi e Ricerche "Enrico Fermi", Rome, Italy
- ¹³ Chicago State University, Chicago, Illinois, USA
- ¹⁴ China Institute of Atomic Energy, Beijing, China
- ¹⁵ Commissariat à l'Energie Atomique, IRFU, Saclay, France
- ¹⁶ COMSATS Institute of Information Technology (CIIT), Islamabad, Pakistan
- ¹⁷ Departamento de Física de Partículas and IGFAE, Universidad de Santiago de Compostela, Santiago de Compostela, Spain
- ¹⁸ Department of Physics and Technology, University of Bergen, Bergen, Norway
- ¹⁹ Department of Physics, Aligarh Muslim University, Aligarh, India
- ²⁰ Department of Physics, Ohio State University, Columbus, Ohio, United States
- ²¹ Department of Physics, Sejong University, Seoul, South Korea
- ²² Department of Physics, University of Oslo, Oslo, Norway
- ²³ Dipartimento di Fisica dell'Università 'La Sapienza' and Sezione INFN Rome, Italy
- ²⁴ Dipartimento di Fisica dell'Università and Sezione INFN, Cagliari, Italy
- ²⁵ Dipartimento di Fisica dell'Università and Sezione INFN, Trieste, Italy
- ²⁶ Dipartimento di Fisica dell'Università and Sezione INFN, Turin, Italy
- ²⁷ Dipartimento di Fisica e Astronomia dell'Università and Sezione INFN, Bologna, Italy
- ²⁸ Dipartimento di Fisica e Astronomia dell'Università and Sezione INFN, Catania, Italy
- ²⁹ Dipartimento di Fisica e Astronomia dell'Università and Sezione INFN, Padova, Italy
- ³⁰ Dipartimento di Fisica 'E.R. Caianiello' dell'Università and Gruppo Collegato INFN, Salerno, Italy
- ³¹ Dipartimento di Scienze e Innovazione Tecnologica dell'Università del Piemonte Orientale and Gruppo Collegato INFN, Alessandria, Italy
- ³² Dipartimento Interateneo di Fisica 'M. Merlin' and Sezione INFN, Bari, Italy
- ³³ Division of Experimental High Energy Physics, University of Lund, Lund, Sweden
- ³⁴ Eberhard Karls Universität Tübingen, Tübingen, Germany
- ³⁵ European Organization for Nuclear Research (CERN), Geneva, Switzerland
- ³⁶ Excellence Cluster Universe, Technische Universität München, Munich, Germany
- ³⁷ Faculty of Engineering, Bergen University College, Bergen, Norway
- ³⁸ Faculty of Mathematics, Physics and Informatics, Comenius University, Bratislava, Slovakia
- ³⁹ Faculty of Nuclear Sciences and Physical Engineering, Czech Technical University in Prague, Prague, Czech Republic
- ⁴⁰ Faculty of Science, P.J. Šafárik University, Košice, Slovakia
- ⁴¹ Faculty of Technology, Buskerud and Vestfold University College, Vestfold, Norway
- ⁴² Frankfurt Institute for Advanced Studies, Johann Wolfgang Goethe-Universität Frankfurt, Frankfurt, Germany
- ⁴³ Gangneung-Wonju National University, Gangneung, South Korea
- ⁴⁴ Gauhati University, Department of Physics, Guwahati, India
- ⁴⁵ Helmholtz-Institut für Strahlen- und Kernphysik, Rheinische Friedrich-Wilhelms-Universität Bonn, Bonn, Germany
- ⁴⁶ Helsinki Institute of Physics (HIP), Helsinki, Finland
- ⁴⁷ Hiroshima University, Hiroshima, Japan
- ⁴⁸ Indian Institute of Technology Bombay (IIT), Mumbai, India
- ⁴⁹ Indian Institute of Technology Indore, Indore (IITI), India
- ⁵⁰ Indonesian Institute of Sciences, Jakarta, Indonesia
- ⁵¹ Inha University, Incheon, South Korea
- ⁵² Institut de Physique Nucléaire d'Orsay (IPNO), Université Paris-Sud, CNRS-IN2P3, Orsay, France
- ⁵³ Institut für Informatik, Johann Wolfgang Goethe-Universität Frankfurt, Frankfurt, Germany
- ⁵⁴ Institut für Kernphysik, Johann Wolfgang Goethe-Universität Frankfurt, Frankfurt, Germany
- ⁵⁵ Institut für Kernphysik, Westfälische Wilhelms-Universität Münster, Münster, Germany
- ⁵⁶ Institut Pluridisciplinaire Hubert Curien (IPHC), Université de Strasbourg, CNRS-IN2P3, Strasbourg, France
- ⁵⁷ Institute for Nuclear Research, Academy of Sciences, Moscow, Russia

- 58 Institute for Subatomic Physics of Utrecht University, Utrecht, Netherlands
59 Institute for Theoretical and Experimental Physics, Moscow, Russia
60 Institute of Experimental Physics, Slovak Academy of Sciences, Košice, Slovakia
61 Institute of Physics, Academy of Sciences of the Czech Republic, Prague, Czech Republic
62 Institute of Physics, Bhubaneswar, India
63 Institute of Space Science (ISS), Bucharest, Romania
64 Instituto de Ciencias Nucleares, Universidad Nacional Autónoma de México, Mexico City, Mexico
65 Instituto de Física, Universidad Nacional Autónoma de México, Mexico City, Mexico
66 iThemba LABS, National Research Foundation, Somerset West, South Africa
67 Joint Institute for Nuclear Research (JINR), Dubna, Russia
68 Konkuk University, Seoul, South Korea
69 Korea Institute of Science and Technology Information, Daejeon, South Korea
70 KTO Karatay University, Konya, Turkey
71 Laboratoire de Physique Corpusculaire (LPC), Clermont Université, Université Blaise Pascal, CNRS–IN2P3, Clermont-Ferrand, France
72 Laboratoire de Physique Subatomique et de Cosmologie, Université Grenoble-Alpes, CNRS-IN2P3, Grenoble, France
73 Laboratori Nazionali di Frascati, INFN, Frascati, Italy
74 Laboratori Nazionali di Legnaro, INFN, Legnaro, Italy
75 Lawrence Berkeley National Laboratory, Berkeley, California, United States
76 Moscow Engineering Physics Institute, Moscow, Russia
77 Nagasaki Institute of Applied Science, Nagasaki, Japan
78 National Centre for Nuclear Studies, Warsaw, Poland
79 National Institute for Physics and Nuclear Engineering, Bucharest, Romania
80 National Institute of Science Education and Research, Bhubaneswar, India
81 National Research Centre Kurchatov Institute, Moscow, Russia
82 Niels Bohr Institute, University of Copenhagen, Copenhagen, Denmark
83 Nikhef, Nationaal instituut voor subatomaire fysica, Amsterdam, Netherlands
84 Nuclear Physics Group, STFC Daresbury Laboratory, Daresbury, United Kingdom
85 Nuclear Physics Institute, Academy of Sciences of the Czech Republic, Řež u Prahy, Czech Republic
86 Oak Ridge National Laboratory, Oak Ridge, Tennessee, United States
87 Petersburg Nuclear Physics Institute, Gatchina, Russia
88 Physics Department, Creighton University, Omaha, Nebraska, United States
89 Physics Department, Panjab University, Chandigarh, India
90 Physics Department, University of Athens, Athens, Greece
91 Physics Department, University of Cape Town, Cape Town, South Africa
92 Physics Department, University of Jammu, Jammu, India
93 Physics Department, University of Rajasthan, Jaipur, India
94 Physik Department, Technische Universität München, Munich, Germany
95 Physikalisches Institut, Ruprecht-Karls-Universität Heidelberg, Heidelberg, Germany
96 Purdue University, West Lafayette, Indiana, United States
97 Pusan National University, Pusan, South Korea
98 Research Division and ExtreMe Matter Institute EMMI, GSI Helmholtzzentrum für Schwerionenforschung, Darmstadt, Germany
99 Rudjer Bošković Institute, Zagreb, Croatia
100 Russian Federal Nuclear Center (VNIIEF), Sarov, Russia
101 Saha Institute of Nuclear Physics, Kolkata, India
102 School of Physics and Astronomy, University of Birmingham, Birmingham, United Kingdom
103 Sección Física, Departamento de Ciencias, Pontificia Universidad Católica del Perú, Lima, Peru
104 Sezione INFN, Bari, Italy
105 Sezione INFN, Bologna, Italy
106 Sezione INFN, Cagliari, Italy
107 Sezione INFN, Catania, Italy
108 Sezione INFN, Padova, Italy
109 Sezione INFN, Rome, Italy
110 Sezione INFN, Trieste, Italy

- 111 Sezione INFN, Turin, Italy
- 112 SSC IHEP of NRC Kurchatov institute, Protvino, Russia
- 113 Stefan Meyer Institut für Subatomare Physik (SMI), Vienna, Austria
- 114 SUBATECH, Ecole des Mines de Nantes, Université de Nantes, CNRS-IN2P3, Nantes, France
- 115 Suranaree University of Technology, Nakhon Ratchasima, Thailand
- 116 Technical University of Košice, Košice, Slovakia
- 117 Technical University of Split FESB, Split, Croatia
- 118 The Henryk Niewodniczanski Institute of Nuclear Physics, Polish Academy of Sciences, Cracow, Poland
- 119 The University of Texas at Austin, Physics Department, Austin, Texas, USA
- 120 Universidad Autónoma de Sinaloa, Culiacán, Mexico
- 121 Universidade de São Paulo (USP), São Paulo, Brazil
- 122 Universidade Estadual de Campinas (UNICAMP), Campinas, Brazil
- 123 University of Houston, Houston, Texas, United States
- 124 University of Jyväskylä, Jyväskylä, Finland
- 125 University of Liverpool, Liverpool, United Kingdom
- 126 University of Tennessee, Knoxville, Tennessee, United States
- 127 University of the Witwatersrand, Johannesburg, South Africa
- 128 University of Tokyo, Tokyo, Japan
- 129 University of Tsukuba, Tsukuba, Japan
- 130 University of Zagreb, Zagreb, Croatia
- 131 Université de Lyon, Université Lyon 1, CNRS/IN2P3, IPN-Lyon, Villeurbanne, France
- 132 Università di Brescia
- 133 V. Fock Institute for Physics, St. Petersburg State University, St. Petersburg, Russia
- 134 Variable Energy Cyclotron Centre, Kolkata, India
- 135 Warsaw University of Technology, Warsaw, Poland
- 136 Wayne State University, Detroit, Michigan, United States
- 137 Wigner Research Centre for Physics, Hungarian Academy of Sciences, Budapest, Hungary
- 138 Yale University, New Haven, Connecticut, United States
- 139 Yonsei University, Seoul, South Korea
- 140 Zentrum für Technologietransfer und Telekommunikation (ZTT), Fachhochschule Worms, Worms, Germany